Geoscientific
Model Development
Discussions

Quantifying and attributing time step sensitivities in present-day climate simulations conducted with EAMv1

Hui Wan[1], Shixuan Zhang[1], Philip J. Rasch[1], Vincent E. Larson[2,1], Xubin Zeng[3], and Huiping Yan[4,1]

[1]Atmospheric Sciences and Global Change Division, Pacific Northwest National Laboratory
[2]Department of Mathematical Sciences, University of Wisconsin – Milwaukee
[3]Department of Hydrology and Atmospheric Sciences, University of Arizona
[4]School of Atmospheric Science, Nanjing University of Information Science and Technology

Correspondence: Hui Wan (Hui.Wan@pnnl.gov)

Abstract. This study assesses the relative importance of time integration error in present-day climate simulations conducted with the atmosphere component of the Energy Exascale Earth System Model version 1 (EAMv1) at 1-degree horizontal resolution. We show that a factor-of-6 reduction of time step size in all major parts of the model leads to significant changes in the long-term mean climate. Examples of such changes include warming in the lower troposphere, cooling in the tropical and subtropical upper troposphere, as well as decreases of relative humidity throughout the troposphere accompanied by cloud fraction decreases. These changes imply that the reduction of temporal truncation errors leads to a notable although unsurprising degradation of agreement between the simulated and observed present-day climate; the model would require retuning to regain optimal climate fidelity in the absence of those truncation errors.

A coarse-grained attribution of the time step sensitivities is carried out by separately shortening time steps used in various components of EAM or by revising the numerical coupling between some processes. Our analysis leads to the counter-intuitive finding that the marked decreases in the subtropical low-cloud fraction and total cloud radiative effect are caused not by the step size used for the collectively subcycled turbulence, shallow convection and stratiform cloud macro- and microphysics parameterizations but by the step sizes used outside the subcycles. Further analysis suggests that the coupling frequency between the subcycles and the rest of EAM has a substantial impact on the marine stratocumulus decks while the deep convection parameterization has a significant impact on trade cumulus. The step size of the cloud macro- and microphysics subcycles appears to have a primary impact on cloud fraction at most latitudes in the upper troposphere as well as in the mid-latitude near-surface layers. Impacts of step sizes used by the dynamical core and radiation appear to be relatively small. These results provide useful clues to help better understand the root causes of time step sensitivities in EAM. The experimentation strategy used here can also provide a pathway for other models to identify and reduce time integration errors.

1 Introduction

Atmospheric General Circulation Models (AGCMs) simulate physical and chemical processes in the Earth's atmosphere by solving a complex set of ordinary and partial differential equations. It is highly desirable that the numerical methods used for solving those equations produce relatively small errors, so that the behavior of an AGCM reflects the inherent characteristics

of the continuous model formulation that describes the model developers' understanding of the underlying physical and chem-
25 ical processes (see, e.g. Beljaars, 1991; Beljaars et al., 2018). However, various studies have shown examples where temporal
discretization methods in AGCMs, especially those used in the parameterization of unresolved processes or in the coupling
between processes, produce large errors that significantly affect key features of the numerical results (Wan et al., 2013; Get-
telman et al., 2015; Beljaars et al., 2017; Donahue and Caldwell, 2018; Zhang et al., 2018; Barrett et al., 2019). These results
are not surprising, given the relatively short time scales associated with parameterized processes such as clouds and turbulence
30 and the relatively long time steps (typically on the order of tens of minutes) used by current global atmospheric GCMs.

This study attempts to take a first step towards assessing and addressing time integration issues associated with physics
parameterizations in the atmospheric component of the U.S. Department of Energy's Energy Exascale Earth System Model
version 1, hereafter referred to as EAMv1 (Rasch et al., 2019). The study contains two parts:

- The first part is an initial assessment of the relative importance of time integration errors in present-day climate simula-
35   tions conducted with EAMv1. This is done by using an intuitive and practical metric, namely the magnitude of changes
in the model's long-term climate resulting from a substantial (in our case a factor of 6) reduction of the time step sizes
used in all major components of the model (e.g., resolved dynamics, parameterized radiation, stratiform clouds, deep
convection, and the numerical coupling of different processes). As we show in Section 3, the consequent changes in
EAMv1's 10-year climate statistics lead to a notable and unsurprising degradation in agreement between the simulations
40   and observations because errors which were previously compensated for using parameter tuning are no longer present in
the model solutions, and no retuning was performed in this study.

- In the second part, a series of sensitivity experiments are conducted and analyzed to identify which components of EAM
are responsible for the changes in cloud fraction and cloud radiative effects. The purpose is to provide clues for future
studies that investigate the root causes of the sensitivities to model time step.

45 The rest of this paper proceeds as follows. Section 2 provides an overview of the EAM model, introduces the time step sizes
used by its main components, and briefly describes the numerical methods used for process coupling. The common setup of the
present-day climate simulations and the methods used for assessing statistical significance of the sensitivities are also described.
Section 3 presents the impact of a proportional, factor-of-6 step size reduction in all major components of EAMv1. Section 4
presents results from additional numerical experiments to attribute the sensitivities in cloud fraction and cloud radiative effects
50 shown in Section 3. The conclusions are drawn in Section 5.

2   Model and simulation overview

2.1   EAMv1

EAMv1 is a global hydrostatic AGCM. The dynamical core solves the so-called primitive equations using a continuous
Galerkin spectral-element method for horizontal discretization on a cubed-sphere mesh (Dennis et al., 2012; Taylor et al.,

55   2009). The vertical discretization uses a semi-Lagrangian approach in a pressure-based terrain-following coordinate (Lin, 2004). Main components of the parameterizations suite include the solar and terrestrial radiation (Mlawer et al., 1997; Iacono et al., 2008), deep convection (Zhang and McFarlane, 1995; Richter and Rasch, 2008; Neale et al., 2008), turbulence and shallow convection (Golaz et al., 2002; Larson et al., 2002; Larson and Golaz, 2005; Bogenschutz et al., 2013), stratiform cloud microphysics (Morrison and Gettelman, 2008a; Gettelman and Morrison, 2015; Gettelman et al., 2015; Wang et al., 2014),
60   aerosol lifecycle and aerosol-cloud interactions (Liu et al., 2016; Wang et al., 2020), and land surface processes (Oleson et al., 2013).

The so-called low-resolution (or standard) configuration of EAM uses a horizontal grid-spacing of approximately 100 km. The vertical grid consists of 72 layers covering an altitude range from the Earth's surface to 0.1 hPa (64 km), with layer thicknesses ranging from 20–100 m near the surface to about 600 m in the free troposphere up to the lower stratosphere. This
65   1-degree configuration is used as one of the workhorses both for model development and in multi-decade simulations targeted at scientific investigations. A more detailed description of EAMv1 can be found in Rasch et al. (2019) and Xie et al. (2018).

Various different time integration methods and time step sizes are used by different parts (hereafter referred to as components) of EAMv1. These are mostly explicit or implicit methods using fixed step sizes. For example, in the dynamical core, the temperature, horizontal winds, and surface pressure equations are advanced in time using an explicit five-stage third-order
70   Runge-Kutta method (Kinnmark and Gray, 1984; Guerra and Ullrich, 2016; Lauritzen et al., 2018). The horizontal tracer advection uses a three-stage second-order strong-stability-preserving Runge-Kutta method (Spiteri and Ruuth, 2002; Guba et al., 2014; Lauritzen et al., 2018). Some parameterizations, e.g., sedimentation of rain and snow and turbulent mixing of aerosols, are subcycled using dynamically determined step sizes.

The primary method used for process coupling isolates a model component representing an atmospheric process or a set of
75   processes within EAM by updating model state variables (e.g., winds, temperature, pressure, and tracer concentrations) that may have been updated by a preceding component. This method is referred to as "time splitting" in Williamson (2002) and in Lauritzen et al. (2018), and is given the name "sequential update splitting" in Donahue and Caldwell (2018). In wider numerical modeling communities, the method is often referred to as "operator splitting" (e.g., Sportisse, 2000). We denote the step size of this splitting/coupling by $\Delta t_{\mathrm{CPLmain}}$. For completeness, it is worth noting that in some parts of EAM, tendencies predicted
80   by one atmospheric process are also passed on to a subsequently calculated process. An example like this can be found in Figure 2b of Zhang et al. (2018) which depicts the coupling between the parameterized physics and the resolved dynamics. These instances of a different process coupling method in the default EAMv1 are not investigated in this study, and hence are not further detailed here. The sequence of calculations used in EAMv1 is schematically depicted in Figure 1a. The following step sizes are used as defaults in the 1-degree configuration of EAMv1:
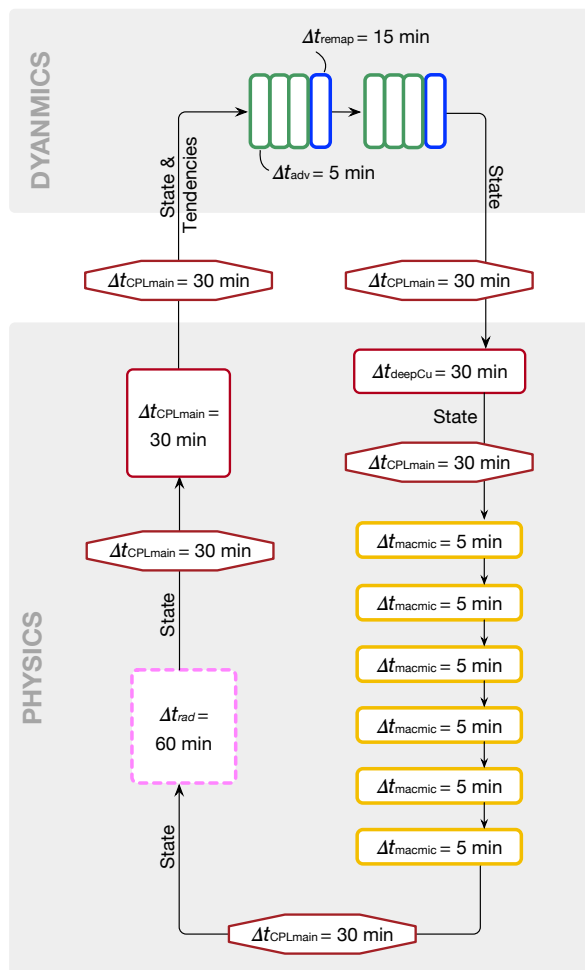
85   – $\Delta t_{\mathrm{CPLmain}}$ = 30 min.

– Within the resolved dynamics, the vertical discretization (remapping) takes step sizes of $\Delta t_{\mathrm{remap}}$= 15 min, each of which is further divided into 3 substeps of Δt_{adv}= 5 min for the horizontal advection of temperature, momentum, and tracers.

(a) Sequence of calculations in EAMv0 and EAMv1
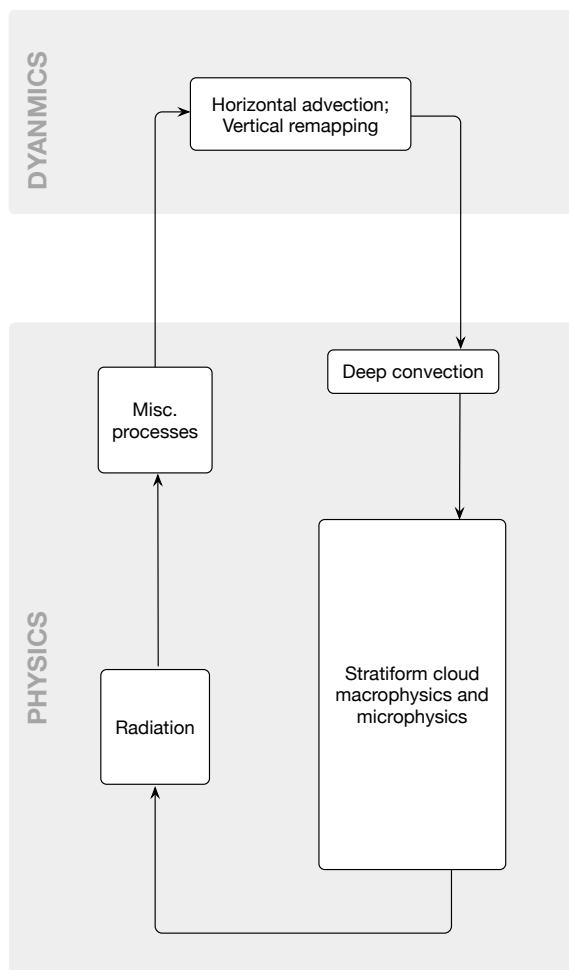
(b) Default time step sizes in EAMv1 (v1_CTRL)

Figure 1. (a) A flowchart showing the sequence of calculations in EAMv1. (b) Time step sizes used in the default EAMv1 for 100 km horizontal resolution (simulation v1_CTRL in this paper). Different colors in panel (b) indicate step sizes controled by different namelist variables in the model source code. Step sizes shown in the same color have the same value. More details can be found in Section 2.1.

These step sizes can be changed independently as long as Δt_{remap} is a multiple of Δt_{adv} and $\Delta t_{\text{CPLmain}}$ is a multiple of Δt_{remap}.

90   – Deep convection uses Δt_{deepCu}= 30 min; this tied to (i.e., has to be the same as) $\Delta t_{\text{CPLmain}}$.

   – The parameterizations of stratiform and shallow cumulus clouds include two elements: (1) a treatment of turbulence and shallow convection named Cloud Layers Unified By Binormals (CLUBB, Golaz et al., 2002; Larson et al., 2002; Larson and Golaz, 2005), which we refer to for brevity as cloud macrophysics in this paper, and (2) a treatment for aerosol activation (formation of cloud liquid and ice particles) and further evolution of cloud condensate which we refer

95   to as cloud microphysics. These two elements are subcycled together using time steps of Δt_{macmic}= 5 min following Gettelman et al. (2015). To facilitate discussions later in this paper, we use the notation $\Delta t_{\text{CPLmacmic}}$ to denote the step size used for coupling the collectively subcycled cloud macro-/microphysics with the rest of EAM. The default EAMv1 has $\Delta t_{\text{CPLmacmic}} \equiv \Delta t_{\text{CPLmain}}$ but an alternative is discussed in Section 4.3. CLUBB can be further subcycled with respect to Δt_{macmic}, but that is not done in either the default EAMv1 or in any of the simulations presented in this paper.

100   – Heating/cooling rates resulting from shortwave (SW) and longwave (LW) radiation are calculated every hour, i.e., Δt_{rad}= 60 min. This means radiation is supercycled with respect to all the other parameterizations as well as the resolved dynamics. During every other time step of $\Delta t_{\text{CPLmain}}$= 30 min when the radiation parameterization is not exercised, the tendencies saved from the previous 30 min time step are used to update the atmospheric state.

   – Miscellaneous other atmospheric processes, e.g., gravity wave drag and the sedimentation, dry deposition, and micro-
105   physics of aerosols, are coupled with each other and with the processes listed above at time intervals tied to $\Delta t_{\text{CPLmain}}$. The coupling to land surface happens at intervals of $\Delta t_{\text{CPLmain}}$ by default; it can be changed to longer multiples of $\Delta t_{\text{CPLmain}}$ but that again is not explored in this study.

These various step sizes are schematically depicted in Figure 1b. Their relationship in the default EAMv1 can be summarized as follows:

$$\Delta t_{\text{CPLmain}} = 2\Delta t_{\text{remap}} = 6\Delta t_{\text{adv}} \tag{1}$$

$$\Delta t_{\text{CPLmain}} \equiv \Delta t_{\text{CPLmacmic}} = 6\Delta t_{\text{macmic}} \tag{2}$$

$$\Delta t_{\text{CPLmain}} \equiv \Delta t_{\text{deepCu}} \tag{3}$$

$$\Delta t_{\text{CPLmain}} = 0.5\Delta t_{\text{rad}}. \tag{4}$$

The equivalent sign ($\equiv$) indicates step sizes that are tied together in the default EAMv1.

2.2   EAMv0

To provide context and serve as a reference for the evaluation of time step sensitivity in EAMv1, we also present one simulation using EAMv0, i.e., EAMv1's most recent predecessor. EAMv0 uses the same dynamical core and large-scale transport

algorithms as in v1, but the vertical grid has only 30 layers. Many of the parameterizations differ from EAMv1. The parameterization of turbulence and shallow convection follows Park and Bretherton (2009), the cloud macrophysics parameterization

120   follows Park et al. (2014), and the cloud microphysics parameterization is described in Morrison and Gettelman (2008b). The time integration methods and step sizes are very similar to those in EAMv1, except that the cloud macro- and microphysics parameterizations are not subcycled (i.e., they use a 30 min step size).

2.3   Present-day climate simulations

A series of 10-year simulations were conducted using an experimental setup commonly exercised in the development and eval-

125   uation of EAM and its predecessors. The model was configured to simulate recent climatological conditions by selecting values of the Earth's orbital conditions, aerosol emissions and greenhouse gas concentrations, land use, and sea surface temperatures and sea ice coverage characteristics of the recent past (around year 2000). The sea surface temperature and sea ice cover were prescribed using monthly climatological values that repeated each year. Prognostic equations were used to produce evolving descriptions of the atmosphere and land states. The simulations used initial conditions written out by a previously performed

130   multiyear simulation. Some of the model configurations used in our sensitivity experiments produced climate statistics that differed substantially from the default configuration; therefore, to avoid characterizing the initial adjustment phase, a 4 month spin-up was performed and neglected in each simulation, and the following 10 years were analyzed.

Simulations were first conducted with EAMv0 or v1 using their default time step sizes. These are labelled "v0_CTRL" and "v1_CTRL", respectively. In a second v1 simulation called "v1_All_Shorter", the various step sizes listed in Eqs. (1)–(4) were

135   proportionally reduced by a factor of 6, cf. Table 1 and flowchart in Figure A1a. This reduction gives a step size of 5 min for most of the parameterizations and for process coupling, which is significantly shorter than the default, but is still practically affordable for sensitivity studies. Results from these three simulations are discussed in Section 3. Additional simulations were also conducted with the v1 model to allow the differences between v1_All_Shorter and v1_CTRL to be attributed to specific sets of processes and time stepping algorithms. The experimental design is summarized in Tables 1 and A1, groups II and III.

140   The attribution process is summarized in Figure 2 with the detailed results discussed in Section 4.

2.4   Statistical tests

The analyses presented in this paper focus primarily on 10-year mean annual averages. To distinguish signals of time step sensitivity from noise caused by natural variability, the two-sample t-test was applied to pairs of simulations conducted with different step sizes, with the test statistic constructed using annual averages. A significance level of 0.05 was chosen to de-

145   termine whether differences between a pair of 10-year averages were statistically significant. This method of two-sample t-test has been used in the diagnostics package of the National Center for Atmospheric Research (NCAR) Atmosphere Model Wording Group (AMWG) who developed predecessors of EAM (http://www.cesm.ucar.edu/working_groups/Atmosphere/ amwg-diagnostics-package/) .

Considering that the sample size of 10 is relatively small, we also conducted statistical testing using monthly mean model

150   output. Serial correlation in monthly averages was addressed by using the paired t-test and the effective sample size (Zwiers

Geoscientific
Model Development
Discussions

Table 1. List of climate simulations conducted in this study. The numbers given in the main part of the table are the ratio of each step size (or $\Delta t_{DeepCu}/\tau$) relative to its value in the default model running at 1-degree horizontal resolution. The meaning and default values of the various Δt values are explained in Section 2. Here τ refers to the prescribed (fixed) time scale in the deep convection parameterization for releasing the convective available potential energy (CAPE), the default value of which is 3600 s. The namelist variables in EAM used to configure these simulations are listed in Table A1. Flowcharts of the EAMv1 simulations are shown in Figures 1, 12, A1, and A2.

| Group | Simulation | Description | Flowchart | Ratio of time step size relative to default | | | | | | | Ratio of $\Delta t_{deepCu}/\tau$ relative to default |
				Δt_{remap}	Δt_{adv}	$\Delta t_{CPLmain}$	Δt_{deepCu}	$\Delta t_{CPLmacmic}$	Δt_{macmic}	Δt_{rad}	
0	v0_CTRL	Sect. 2.2	-	1	1	1	1	1	1	1	1
I	v1_CTRL	Sect. 2.1	Fig. 1	1	1	1	1	1	1	1	1
I	v1_All_Shorter	Sect. 2.3	Fig. A1a	1/6	1/6	1/6	1/6	1/6	1/6	1/6	1/6
II	v1_MacMic_Shorter	Sect. 4.1	Fig. A1b	1	1	1	1	1	1/6	1	1
II	v1_All_Except_MacMic_Shorter	Sect. 4.1	Fig. A2a	1/6	1/6	1/6	1/6	1/6	1	1/6	1/6
III	v1_CPL+DeepCu_Shorter	Sect. 4.3.1	Fig. A2b	1/3	1	1/6	1/6	1/6	1	1	1/6
III	v1_CPL+DeepCu+Tau_Shorter	Sect. 4.3.3	Fig. A2b	1/3	1	1/6	1/6	1/6	1	1	1
III	v1_Dribble	Sect. 4.3.2	Fig. 12	1	1	1	1	1/6	1	1	1
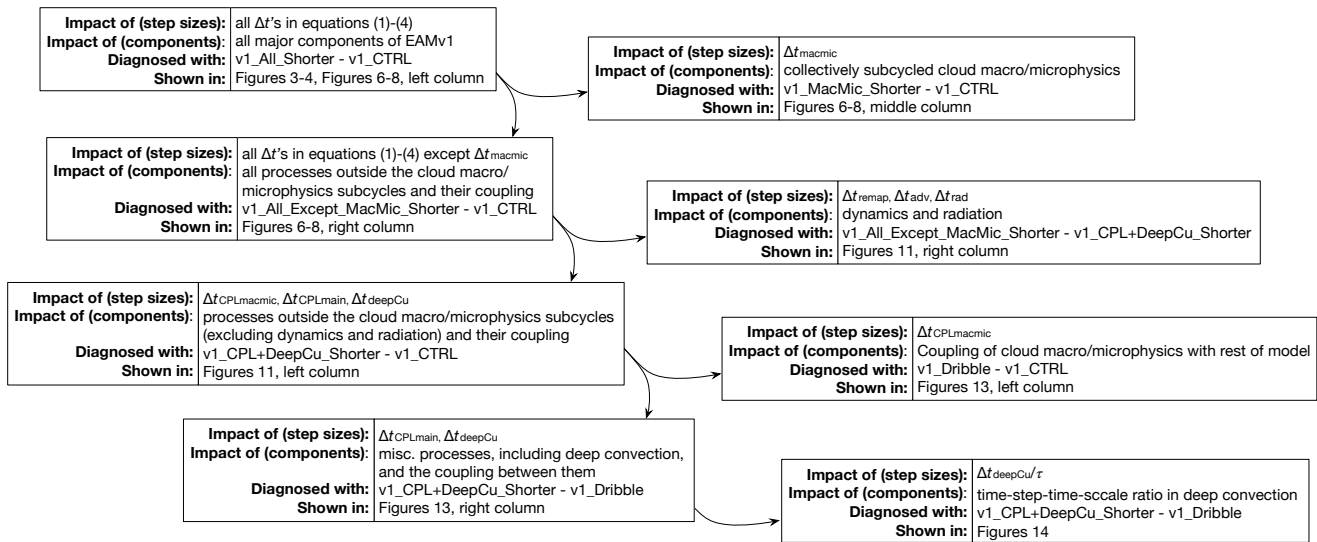
Figure 2. Schematic showing the attribution of time step sensitivities using simulations listed in Tables 1 and A1. Flowcharts of the simulations are shown in Figures 1, 12, A1, and A2.

and von Storch, 1995). For example, to assess the significance of the differences between simulations A and B at a certain geographical location, we used the time series of monthly mean $A - B$ (which had 120 data points in the monthly time series) to construct the test statistic for a one-sample t-test, taking into account the autocorrelation in the time series. A significance level of 0.05 was chosen to determine whether the mean of the differences was statistically zero.

155   We processed all the difference plots shown in the paper using both methods. The two methods turned out to give rather consistent results overall. They disagree only at a small portion of grid points associated with relatively small climate differences. The key signatures of time step sensitivity discussed below were considered statistically significant by both methods. We chose to show results from the two-sample test in the paper to be consistent with the AMWG diagnostics package.

3   Impact of proportional step size reductions in all major processes

160   The first question we attempt to answer is whether the characteristics of EAMv1's present-day climate are substantially affected by the choices of time step sizes. This is done by comparing simulations v1_CTRL and v1_All_Shorter. To put the magnitude of the differences into context, we also show some representative results from v0_CTRL.

3.1   Time step sensitivities in EAMv1

It turns out that the proportional factor-of-6 step size reduction in all major components of the v1 model leads to systematic
165   changes in the simulated long-term climate. In the middle column of Figure 3, the differences in 10-year-mean zonal averages
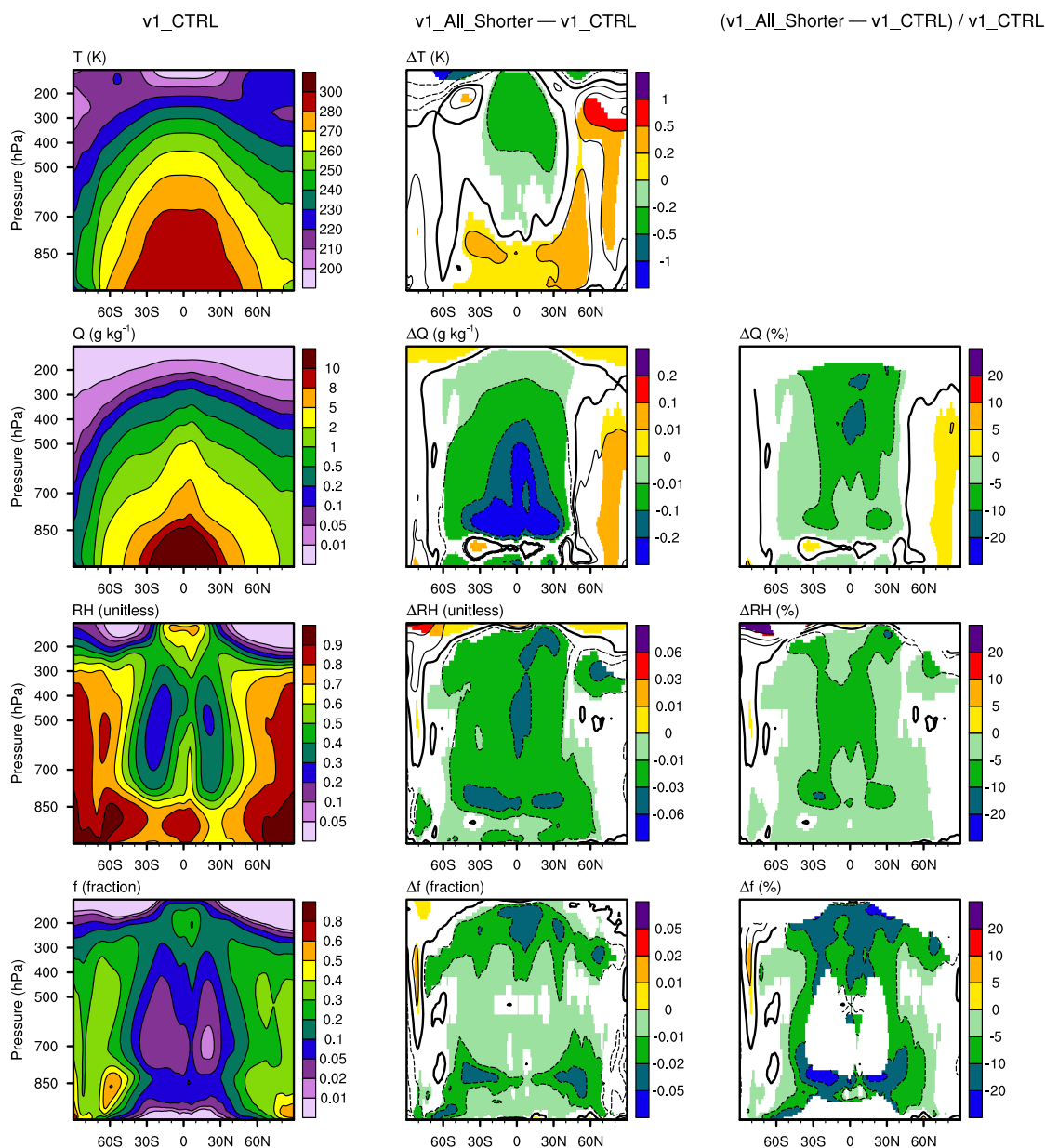
Figure 3. Left column: 10-year mean, zonally averaged air temperature (T), specific humidity (Q), relative humidity (RH), and cloud fraction (f) in simulation v1_CTRL. Middle column: differences between v1_All_Shorter and v1_CTRL. Right column: relative differences with respect to v1_CTRL. Statistically insignificant differences are masked out in white. The simulation setups are described in Section 2.3, Table 1 and Table A1, group I. The flowcharts can be found in Figures 1 and A1a.
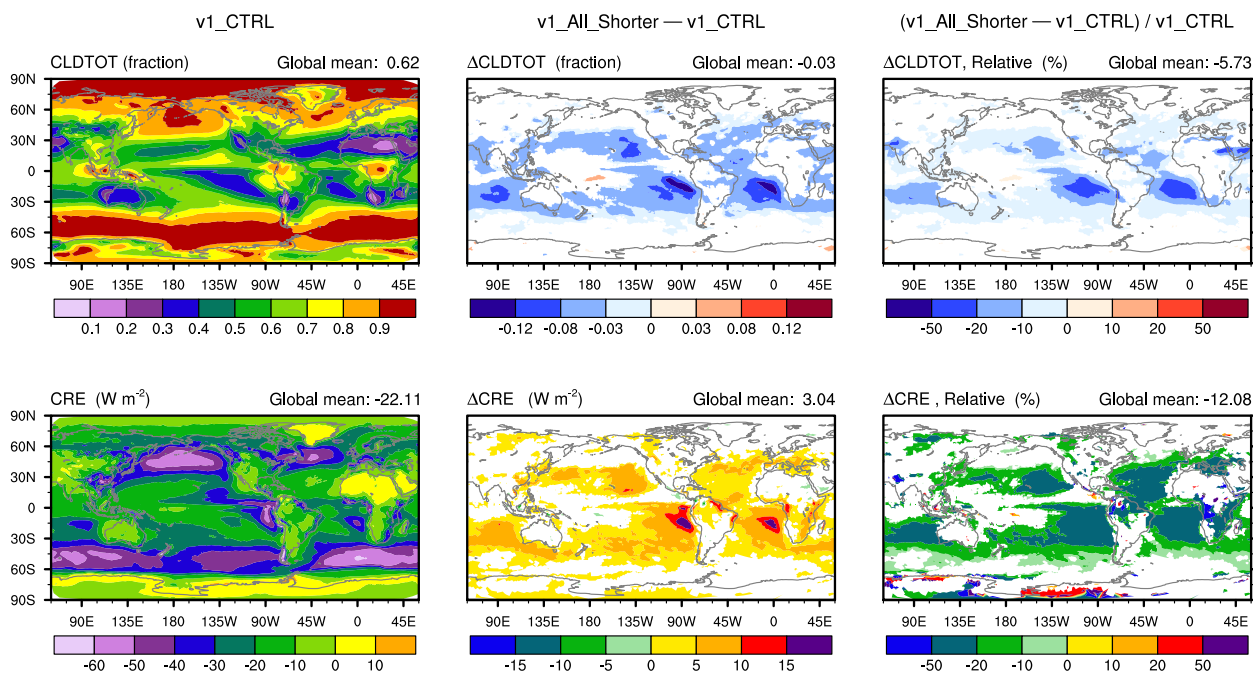
Figure 4. Left column: 10-year mean geographical distribution of total cloud cover (CLDTOT, upper row) and total cloud radiative effect (CRE, lower row) in v1_CTRL. Middle column: differences between v1_All_Shorter and v1_CTRL. Right column: relative differences with respect to v1_CTRL. Statistically insignificant differences are masked out in white. The simulation setups are described in Section 2.3, Table 1, and Table A1, group I. The flowcharts can be found in Figures 1 and A1a.

between v1_All_Shorter and v1_CTRL are shown for air temperature (T), specific humidity (Q), relative humidity (RH) and cloud fraction (f). The relative differences normalized by the corresponding values in v1_CTRL are shown in the right column. (Relative differences in T are not a useful measure and hence not included.) Statistically *insignificant* differences are masked out in white. The figure reveals that the step size reduction leads to warming of up to 0.5 K in the subtropical and mid-latitude

170 near-surface layers and cooling of similar magnitudes in the tropical mid- and upper-troposphere (Figure 3, second panel in first row). In the middle and low latitudes, the air dries at most altitudes in the troposphere, showing typical decreases of 1% to 10% in both specific and relative humidity (Figure 3, right column). Cloud fraction also decreases (Figure 3, bottom row). The largest changes appear in three regions: in the upper troposphere where ice clouds dominate, in the subtropical lower troposphere where stratocumulus and trade cumulus prevail, and in the mid-latitude near-surface layers.

175 The 10-year mean geographical distribution of total cloud cover and total cloud radiative effect (CRE) are shown in Figure 4. Here the signatures of time step sensitivity appear to be dominated by changes in subtropical stratocumulus and trade cumulus clouds over the oceans. The largest local changes are on the order of -10% to -50% for cloud cover and -20% to -50% for CRE. The global mean CRE weakens by about 3 W m^{-2}, corresponding to a relative change of -12%.

Geoscientific
Model Development
Discussions

EGU

3.2 Comparison with observations and EAMv0

180 A recent evaluation of EAMv1 has shown that the simulated present-day climate is cooler and drier than reanalysis in the tropical upper troposphere while the CRE in the major marine stratocumulus regions are weaker compared to satellite products (cf. Figures 3, 4, and 10 in Rasch et al., 2019). Comparing those results with the time step sensitivities shown in Figures 3 and 4, one gets the impression that model biases in v1_All_Shorter are likely to be larger than those in v1_CTRL. Here a model bias is defined as a deviation from the real-world observation. To obtain a comprehensive and yet concise assessment of the impact

185 of time step sizes on model fidelity, we follow the spirit of Donahue and Caldwell (2018) and use the collection of reanalyses and satellite products listed in Table 5 to evaluate the fidelity of v1_CTRL and v1_All_Shorter. The results are presented in Figure 5, where the upper panel shows the relative errors in the simulated global averages and the lower panel shows the relative errors in global patterns. The relative pattern error is defined as the centered root-mean-square (RMS) difference between the simulated and observed patterns, normalized by the RMS of the observed pattern. A "pattern" here refers to the annual mean,

190 global, geographical distribution of a physical quantity. The model results used in the calculations were 10-year averages. The observational data was averaged over the years indicated in Table 5. The biases in v0_CTRL are also included in the figure for comparison.

Figure 5 reveals that model biases in both the global mean (upper panel) and the spatial pattern (lower panel) are larger in v1_All_Shorter for most of the physical quantities examined here; the magnitude of the differences is comparable to the differ-

195 ences between v1_CTRL and v0_CTRL. For clarification, we note that v1_CTRL and v0_CTRL have different characteristic biases due to the substantial changes in the parameterizations and the vertical resolution. For example, Figure A3 shows that the shortwave CRE biases in the low latitudes are dominated by overestimation in the monsoon regions in v0 and underestimation associated with the marine stratocumulus decks and over the warm pool. If we were to compare the local differences between v1_All_Shorter and v1_CTRL with the local differences between v0_CTRL and v1_CTRL, then the time step caused

200 differences will appear to be substantially smaller than the differences caused by changes in parameterizations and vertical resolution, as should be expected. On the other hand, when comparing all three simulations (v1_All_Shorter, v1_CTRL, and v0_CTRL) with observations, we see that the degradation of model fidelity caused by reducing step sizes in v1 has a magnitude similar to the fidelity differences between v1_CTRL and v0_CTRL.

Given that substantial efforts have been made to tune the default EAMv1, i.e., to adjust the values of uncertain parameters

205 in the model's equations in order to improve the match between the simulations and observations (see, e.g., Xie et al., 2018; Rasch et al., 2019), a degradation of model fidelity associated with shortened time steps is not surprising. Assuming the time integration methods used in EAMv1 are mathematically consistent and convergent, one would expect shorter time steps to give *numerically* more accurate results. The results shown in Figure 5 indicate that the default EAMv1 contains sizable time integration errors that are compensated by parameter tuning or by other sources of model error. While the existence of

210 compensating errors is undesirable, it seems to be the widely recognized and accepted status quo. Reducing time integration errors would sacrifice the immediate results and temporarily degrade model fidelity, but it would also provide the opportunity to first expose and then address errors from other sources, hence eventually leading to a model that gives correct results for correct

Table 2. List of observational data and EAM's output used for evaluating the model biases. The observational data were obtained from NCAR AMWG diagnostics package (http://www.cgd.ucar.edu/amp/amwg/diagnostics/plotType.html).

Physical quantity	Source of observation	EAM output
Surface longwave downwelling flux	ISCCP (1983–2000)	FLDS
Surface net longwave flux	ISCCP (1983–2000)	FLNS
TOA upward longwave flux	CERES-EBAF (2000–2010)	FLUT
TOA clearsky upward longwave flux	CERES-EBAF (2000–2010)	FLUTC
TOA longwave cloud forcing	CERES-EBAF (2000–2010)	LWCF
Surface net shortwave flux	ISCCP (1983–2000)	FSNS
TOA net shortwave flux	CERES-EBAF (2000–2010)	FSNTOA
TOA clearsky net shortwave flux	CERES-EBAF (2000–2010)	FSNTOAC
Shortwave cloud radiative effect	CERES-EBAF (2000–2010)	SWCF
Total cloud amount	CloudSat (2007–2010)	CLDTOT
200 hPa zonal wind	JRA25 (1979–2004)	U
500 hPa geopotential height	JRA25 (1979–2004)	Z3
Precipitation rate	GPCP (1979–2009)	PRECT
Total precipitable water	NVAP (1988–1999)	TMQ
Sea level pressure	ERAI (1989–2005)	PSL
Surface latent heat flux	JRA25 (1979–2004)	LHFLX
Surface sensible heat flux	JRA25 (1979–2004)	SHFLX
Surface stress	ERS (1992–2000)	TAUX, TAUY
2m air temperature	LEGATES (1920–1980)	TREFHT
Sea level temperature on land	NCEP (1979–1998)	TS

reasons. As a first step towards reducing time-stepping errors in EAMv1, the next section identifies the model components that have caused the differences between v1_All_Shorter and v1_CTRL. While a number of physical quantities are shown in

215 Figure 5, the analysis in the remainder of the paper focuses on cloud fraction and CRE. Extension of the analysis to additional variables, such as temperature, humidity, precipitation, and winds, are left to future studies.

4 Attributing time step sensitivities in cloud fraction and CRE

The primary method used here for attributing the differences between v1_All_Shorter and v1_CTRL is to carry out sensitivity experiments in which we vary the step sizes used by different subsets of EAM's components. These experiments are sum-

220 marized in Tables 1 and A1, groups II and III, and are described in detail in the following subsections. An overview of the attribution process is provided in Figure 2 with pointers to the figures.
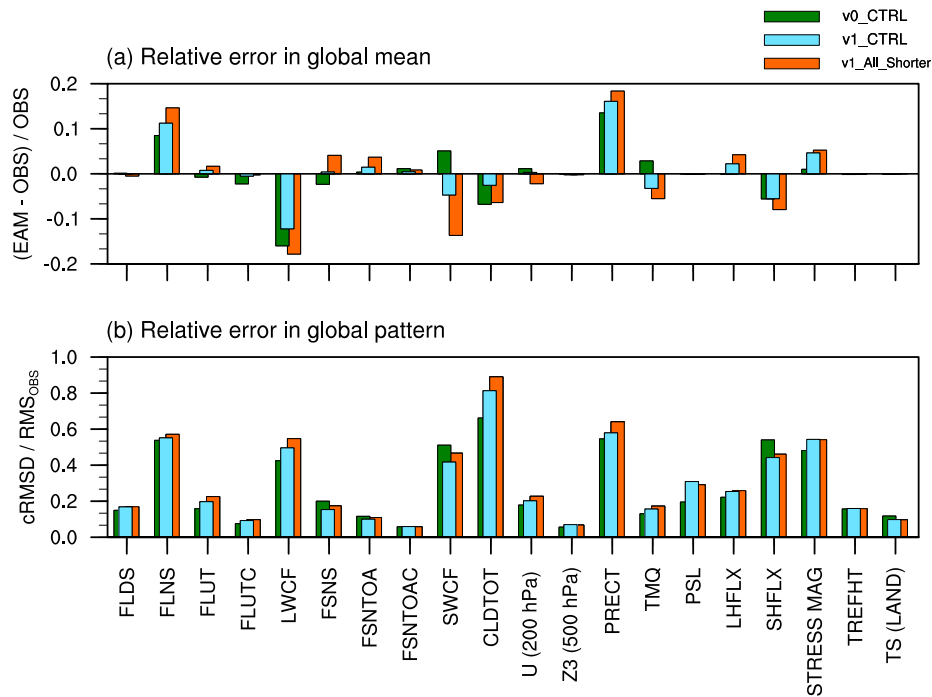
Figure 5. Comparison of 10-year-mean climate simulated by v1_All_Shorter, v1_CTRL and v0_CTRL with various reanalyses and satellite products. The upper panel shows relative errors in the simulated global averages. The lower panel shows the relative error in the simulated geographical distributions, as measured by the centered root-mean-square differences (cRMSD) between model results and the observations normalized by the root-mean-square of the observed global distribution (RMS$_{OBS}$). The long names of the physical quantities labeled along the x-axis are listed in Table 2 together with the sources of observational data.

4.1 Stratiform cloud parameterizations versus the rest of EAMv1

The key signatures in the total cloud cover and CRE changes are seen in the subtropics where marine stratocumulus and trade cumulus are the dominant cloud types (Figure 4). Since these clouds are strongly affected by turbulence, shallow convec-
225 tion, and microphysics, it seems natural to link those changes with the corresponding parameterizations. Two hypotheses are explored here:

- Hypothesis 1: The differences in total cloud cover and CRE seen in the subtropics between v1_All_Shorter and v1_CTRL are caused by time integration errors in the stratiform and shallow cumulus cloud macro- and microphysics parameterizations, i.e., CLUBB, aerosol activation, and MG2. Turbulence and cloud microphysics are known to have relatively
230 short characteristic time scales. The 5 min step size ($\Delta t_{\mathrm{macmic}}$= 5 min) used in the default EAMv1 cannot sufficiently resolve those short time scales and hence gives numerically inaccurate results.

- – Hypothesis 2: The differences in total cloud cover and CRE seen in the subtropics between v1_All_Shorter and v1_CTRL are caused by time integration errors in parts of EAM other than the cloud macro- and microphysics parameterizations or in process coupling. In v1_All_Shorter, the reduction of time integration error in those other components or their coupling with cloud macro- and microphysics results in a different atmospheric environment being provided to CLUBB, and hence triggering different responses of the shallow cumulus and stratiform clouds.

The two sensitivity experiments listed in group II of Tables 1 and A1 were carried out to investigate these hypotheses: Simulation **v1_MacMic_Shorter** (see also flowchart in Figures A1b) sets the step size of the collectively subcycled shallow cumulus and stratiform cloud parameterizations, i.e., CLUBB, aerosol activation, and MG2, to 1/6 of the default value, i.e., Δt_macmic = 5/6 min as in v1_All_Shorter. The rest of EAMv1 used the identical time integration strategy (and thus equivalent time step sizes) as in v1_CTRL. In other words, within each of the main coupling time step $\Delta t_\mathrm{CPLmain}$ = 30 min, instead of 6 invocations of the cloud macro- and microphysics parameterizations with 5 min time steps, there were 36 invocations with 5/6 min time steps. The differences between results from v1_MacMic_Shorter and v1_CTRL are attributed to differences in Δt_macmic which controls the step sizes used in CLUBB and MG2 as well as the interactions between the processes within each subcycle.

Simulation **v1_All_Except_MacMic_Shorter** (see also flowchart in Figure A2a) has the opposite setup, i.e., Δt_macmic= 5 min as in v1_CTRL while the rest of EAMv1 used the much shorter steps as in v1_All_Shorter. The differences in model climate between v1_All_Except_MacMic_Shorter and v1_CTRL are attributed to reduced step sizes for all model components outside the cloud macro- and microphysics subcycles and for the coupling (i.e., information exchange) between the subcycles and the other components (cf. Eqs. (1)–(4)).

The 10-year mean difference plots shown in Figures 6–8 indicate that the changes in long-term climate caused by Δt_macmic and other step sizes are both non-negligible but show different signatures. The zonal mean temperature, humidity, and cloud fraction differences shown Figure 6 reveal that:

- – The warming as well as decreases in cloud fraction *around 850 hPa in the subtropics* (Figure 6a and j) is primarily attributable to shorter step sizes *outside* the cloud macro- and microphysics subcycles (Figure 6, right column);

- – The cooling, drying, and cloud fraction decreases in the *tropical middle and upper troposphere* (Figure 6, left column) are attributable to shortened Δt_macmic (Figure 6, middle column) ;

- – The decreases in cloud fraction in the *mid-latitude near-surface layers* are also attributable to shortened Δt_macmic (Figure 6j and k).

Geographical distributions of high-cloud and low-cloud fraction changes are shown in Figure 7. The corresponding LW, SW, and total CRE changes are shown in Figure 8. Consistent with the signatures seen in the pressure-latitude cross-sections in Figure 6, one can see the major impact of Δt_macmic on high-cloud fraction (Figure 7 top row) and LWCRE (Figure 8 top row). The step sizes outside the cloud macro- and microphysics subcycles play a major role in affecting the low-cloud fraction (Figure 7 second row) and SWCRE (Figure 8 second row). Although reductions in the various step sizes all lead to weakening of
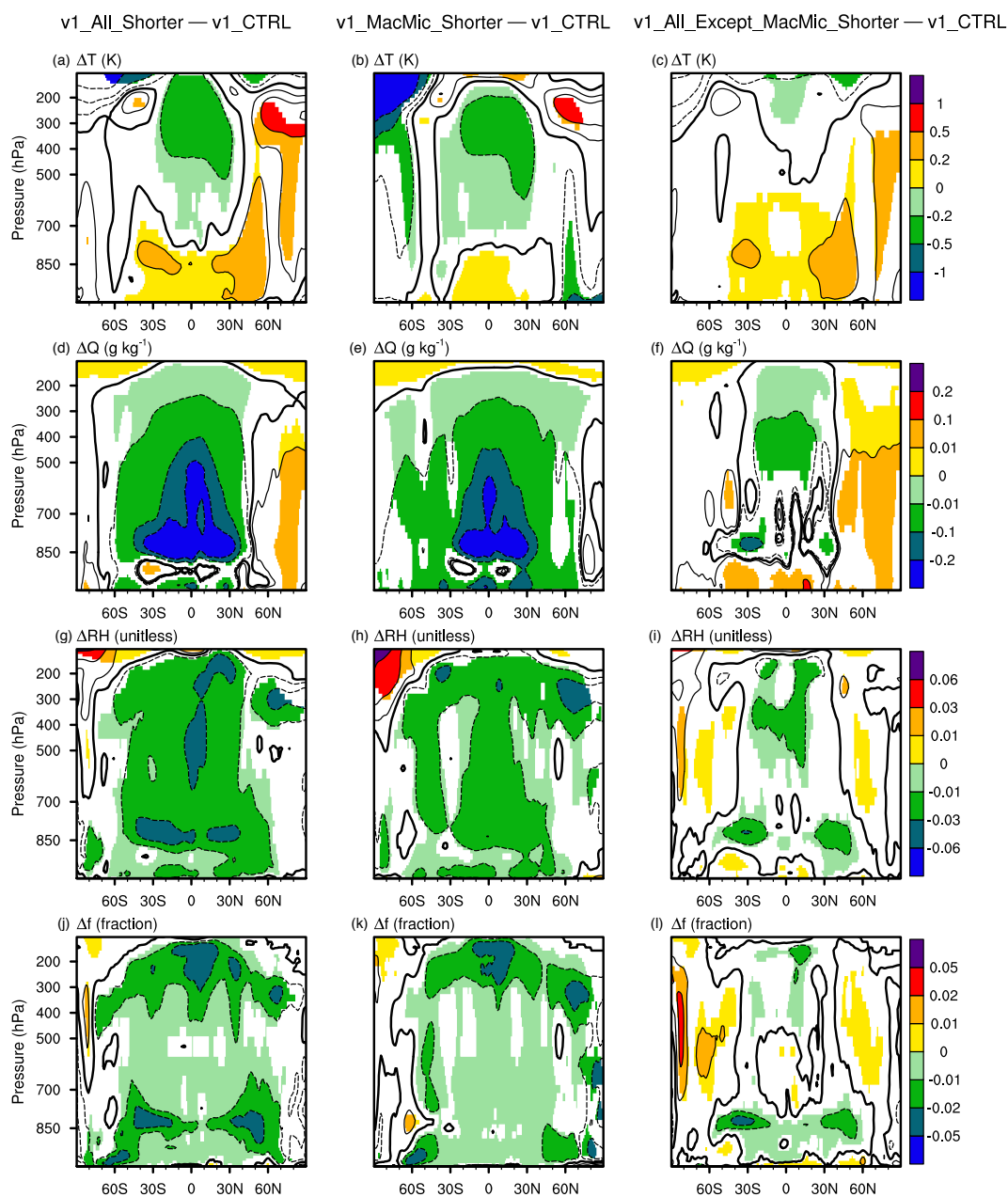
Figure 6. Differences in 10-year mean, zonally averaged air temperature (T), specific humidity (Q), relative humidity (RH), and cloud fraction (f) between various simulations. Left column: v1_All_Shorter - v1_CTRL; middle column: v1_MacMic_Shorter - v1_CTRL; right column: v1_All_Except_MacMic_Shorter - v1_CTRL. Statistically insignificant differences are masked out in white. The simulation setups are described in Section 2.3, Table 1, and Table A1. The flowcharts can be found in Figures 1, A1, and A2a.
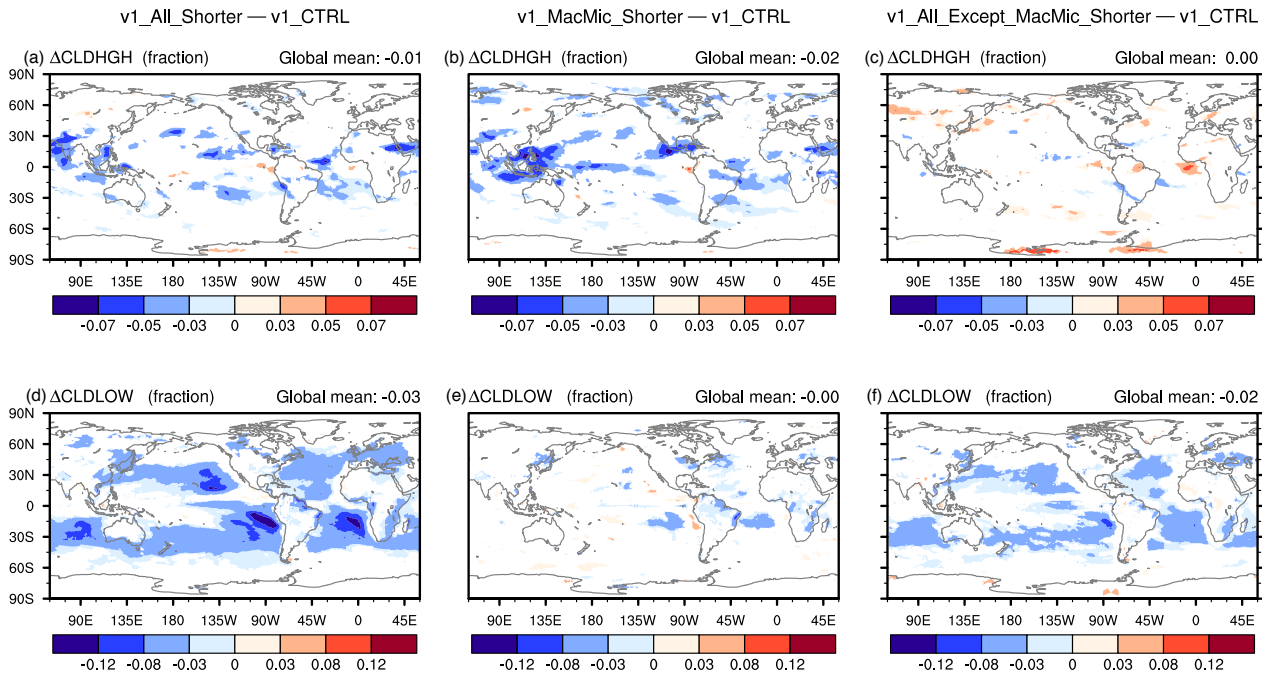
Figure 7. Geographical distribution of 10-year mean differences in high-cloud fraction (CLDHGH, upper row) and low-cloud fraction (CLD-LOW, bottom row). Left column: differences between v1_All_Shorter and v1_CTRL revealing the impact of shortening all major time steps listed in Eqs. (1)-(4); middle column: differences between v1_MacMic_Shorter and v1_CTRL revealing the impact of shortening time steps for the subcycled cloud macro- and microphysics parameterizations; right column: differences between v1_All_Except_MacMic_Shorter and v1_CTRL revealing the impact of shortening step sizes outside the cloud macro- and microphysics subcycle. Statistically insignificant results are masked out in white. The simulation setups are described in Section 2.3, Table 1, and Table A1. The flowcharts can be found in Figures 1, A1, and A2a.

both LWCRE and SWCRE, the total CRE changes seen in Figure 8g are dominated by the SW changes attributable to reduced low-cloud fractions associated with shorter time steps outside the cloud macro- and microphysics subcycles (Figures 8f and Figure 7f).

These results are rather counter-intuitive at first glance. Since the topical upper troposphere is strongly affected by deep convection and the resulted detrainment of water vapor and cloud condensate, one might have assumed the sensitivities in these regions to be caused primarily by step sizes associated with the deep convection parameterization – or dynamics and other processes that introduce atmospheric instability which in turn triggers deep convection. Yet the results shown in Figures 6 and 7 suggest that the cloud fraction decreases in these regions are caused by shortening $\Delta t_{\mathrm{macmic}}$, the step size used by turbulence, shallow convection, and stratiform clouds. A separate study has found evidence that the sensitivities in the tropical upper troposphere have to do with the representation of ice cloud microphysics in EAM. The details will be reported in a different
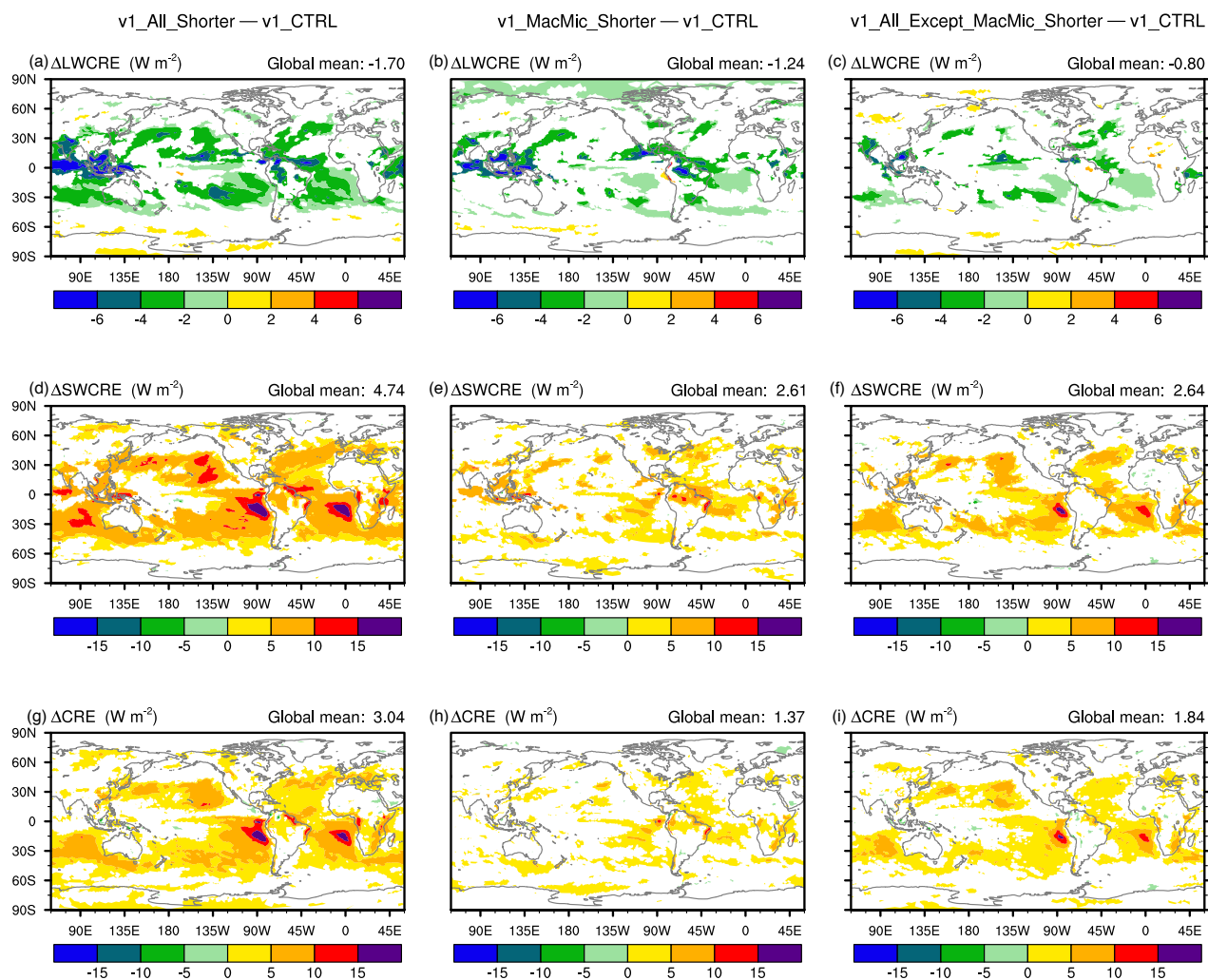
Figure 8. As in Figure 7, but showing the longwave (LW, top row), shortwave (SW, middle row), and total (bottom row) CRE.

275 paper and hence not elaborated here. The link between mid-latitude near-surface clouds and $\Delta t_{\mathrm{macmic}}$ is unclear and needs further exploration.

The results shown in Figures 6–8 lead to the conclusion that step sizes used outside the cloud macro- and microphysics subcycles are more impactful than the step size of the subcycles (i.e., $\Delta t_{\mathrm{macmic}}$) in terms of the sensitivities they cause in cloud fraction and total CRE of the subtropical low clouds. This is also counter-intuitive, and suggests that the low-cloud
280 differences between v1_All_Shorter and v1_CTRL reflect responses of the subcycled processes to changes in the atmospheric environment passed into the subcyles. In other words, hypothesis 2 is valid for the subtropical low clouds. Next, we demonstrate in Section 4.2 that those low-cloud changes are associated with changes in the thermodynamic (instead of dynamic) features of the atmospheric environment. In Section 4.3, additional sensitivity experiments are presented to further attribute these changes to specific processes and step sizes in the rest of EAMv1.

285 ## 4.2 Dynamic versus thermodynamic responses of the subtropical climate

Large-scale subsidence is one of the key features of the subtropical climate. To find out whether the reduced low-cloud fraction and weaker CRE in v1_All_Shorter are associated with weakened subsidence, the method from Bony et al. (2004) is used to compare the dynamic and thermodynamic components of the low-cloud changes.

We first examined the geographical distribution of grid-resolved vertical velocity ω at 500 hPa; the differences among the
290 various simulations discussed so far appeared to be rather small and statistically insignificant and hence are not shown here. This conclusion can also be inferred from the frequency of occurrence of 500 hPa ω, denoted here as P_ω, shown in Figure 9. P_ω here is diagnosed using monthly-mean grid-point-by-grid-point ω values in the latitude band of 35°S to 35°N. The solid black line in Figure 9 is P_ω in v1_CTRL; the dashed color lines show differences in P_ω between other simulations and v1_CTRL. The differences appear to be close to zero compared to P_ω in v1_CTRL.
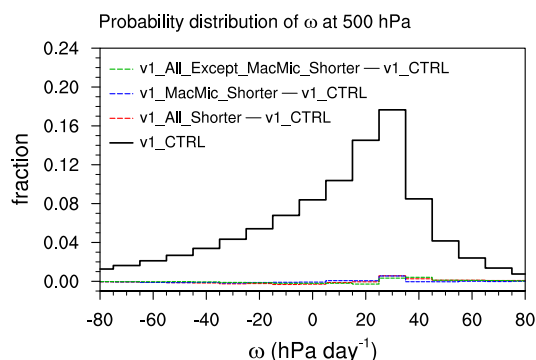
Figure 9. Frequency of occurrence of circulation regimes defined by monthly-mean 500 hPa vertical velocity (ω) in the latitude band of 35°S–35°N. Solid black line shows the probability distribution in v1_CTRL. Dashed color lines show differences in the probability distribution between other simulations and v1_CTRL.

Geoscientific
Model Development
Discussions
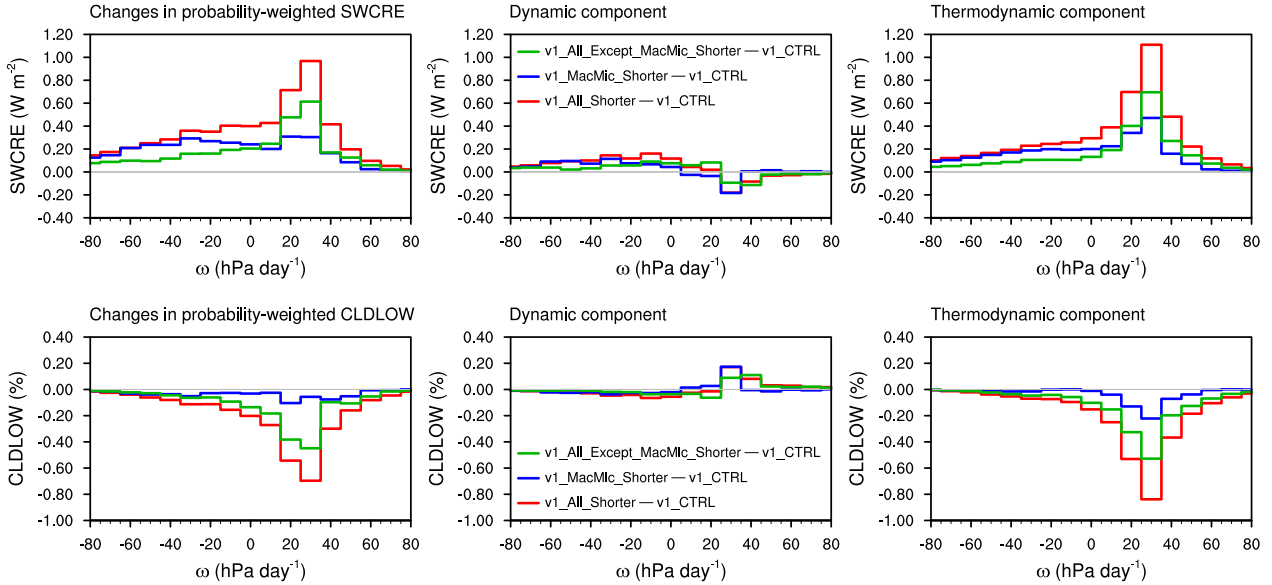
Figure 10. Left column: changes in the probability-weighted SWCRE (upper row) and low-cloud fraction (lower row) in circulation regimes characterized by grid-resolved 500 hPa ω (cf. definitions in Eqs. 5 and 6). Middle and right columns: the dynamic and thermodynamic components of the changes (cf. Eq. 6). Details of the analysis can be found in Section 4.2.

295   We then followed Bony et al. (2004) and defined circulation regimes using monthly mean ω. For a circulation regime associated with ω values between ω_1 and ω_2, we refer to the integral of a generic physical quantity ψ weighted by the probability density function $p(\omega)$ as the probability-weighted ψ, i.e.,

$$\psi_{(\omega_1,\omega_2)} = \int_{\omega_1}^{\omega_2} \psi\, p(\omega)\, d\omega\,. \tag{5}$$

Following Bony et al. (2004), changes in the probability-weighted ψ can be decomposed as follows:

300    $$\Delta\psi_{(\omega_1,\omega_2)} \quad \approx \quad \underbrace{\int_{\omega_1}^{\omega_2} \psi\, \Delta[p(\omega)]\, d\omega}_{\text{dynamic}} + \underbrace{\int_{\omega_1}^{\omega_2} (\Delta\psi)\, p(\omega)\, d\omega}_{\text{thermodynamic}} + \underbrace{\int_{\omega_1}^{\omega_2} (\Delta\psi)\, \Delta[p(\omega)]\, d\omega}_{\text{covariation}} \tag{6}$$

In Figure 10, we present changes in the probability-weighted low-cloud fraction and SWCRE in the left column and the decomposition in the middle and right columns. The results suggest that the low-cloud and SWCRE changes in regions associated with subsidence can be attributed primarily to the thermodynamic responses of the model atmosphere instead of vertical velocity changes.

19

4.3 Further attribution of subtropical low-cloud changes

In earlier sections, it has been shown that the reduction in subtropical marine low-cloud fraction and CRE in v1_All_Shorter are caused primarily by the use of shorter time steps for model components outside the cloud macro- and microphysics subcycles and for the coupling (i.e., information exchange) between the subcycles and the other components. We now make an attempt to refine the granularity of the attribution. Additional sensitivity experiments are discussed in this subsection and summarized as group III in Tables 1 and A1. Schematics of the new simulations are shown in Figure A2b and Figure 12. An overview of the attribution process is provided in Figure 2 with pointers to the figures.

4.3.1 Resolved dynamics and radiation

A simulation was configured similar to v1_All_Except_MacMic_Shorter but with some aspects of the model step sizes returned to values closer to v1_CTRL. Specifically, the horizontal advection time step (Δt_{adv}) in the dynamical core was set to 5 min and the frequency of the radiation calculation Δt_{rad} was set to 60 min, both the same as in v1_CTRL. On the other hand, $\Delta t_{\mathrm{CPLmain}}$ (which controls the step sizes of deep convection, gravity wave drag, various aerosol processes, exchanges with surface models, and the coupling between these processes as well as between physics and dynamics) was set to the smaller value of 5 min. The subcycled cloud macro- and microphysics used time steps of 5 min as in v1_CTRL but was coupled with the rest of the model more frequently (i.e., every 5 min). Because of the required relationship among $\Delta t_{\mathrm{remap}}$, Δt_{adv} and $\Delta t_{\mathrm{CPLmain}}$ (cf. Section 2), this new simulation ended up using a value of $\Delta t_{\mathrm{remap}}$ in between what were used in v1_CTRL and v1_All_Except_MacMic_Shorter, but the impact is expected to be small. This new experiment is referred to as **v1_CPL+DeepCu_Shorter** (cf. Table 1 and Figure A2b); it differs from v1_All_Except_MacMic_Shorter in its larger (i.e., reverted to EAMv1 default) values of Δt_{adv} and Δt_{rad}.

The CRE differences between this new experiment and v1_CTRL, displayed in the left column of Figure 11, show strong similarity to the rightmost panel of Figure 8. In contrast, the impact of dynamics and radiation time steps, indicated by the CRE differences between v1_All_Except_MacMic_Shorter and this new experiment (Figure 11, right column), appears to have small and mostly insignificant magnitudes. The small yet systematic differences in LWCRE in the Southern Hemisphere midlatitudes (Figure 11b) indicate a shift in the location of the storm tracks, but no systematic signals are seen in the lower latitudes. Therefore we conclude that the impact of dynamics and radiation time steps on subtropical clouds is small, at least in the context of the currently used process ordering and splitting/coupling methods.

### 4.3.2 Coupling between cloud macro/microphysics and other processes

We are now left with two time step sizes to explore, $\Delta t_{\mathrm{CPLmain}}$ and $\Delta t_{\mathrm{deepCu}}$. As explained in Section 2 and illustrated by color coding in the flowcharts, these two step sizes have the same value in EAMv1, and the single $\Delta t_{\mathrm{CPLmain}}$ also controls the coupling frequency among the majority of the parameterizations as well as between physics and dynamics. This makes further attribution somewhat difficult unless changes are made to the model source code. Nevertheless, our exploration revealed that the coupling between the subcycled cloud parameterizations and the rest of the model was impactful. This can be demonstrated
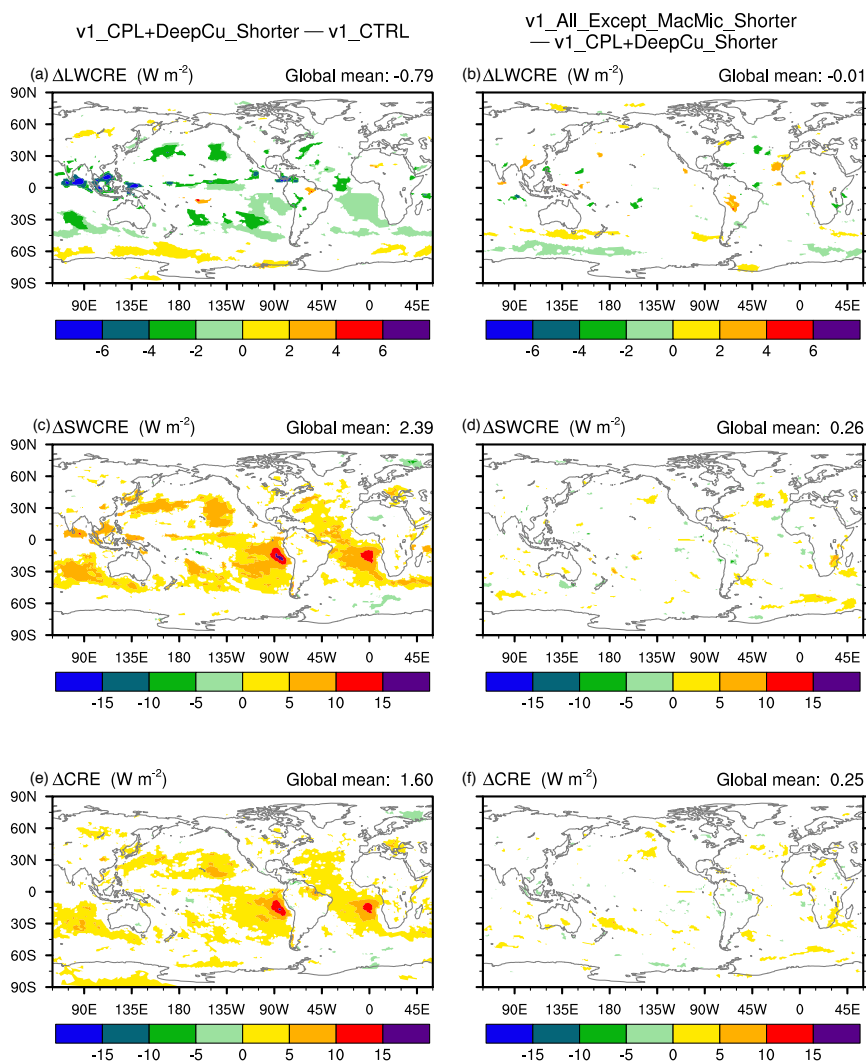
Figure 11. Attribution of the 10-year mean CRE differences shown in the rightmost column of Figure 8. Left: CRE differences between v1_CPL+DeepCu_Shorter and v1_CTRL revealing the impact of step sizes used for process coupling/splitting and deep convection. Right: CRE differences between v1_All_Except_MacMic_Shorter and v1_CPL+DeepCu_Shorter revealing the impact of dynamics and radiation time steps. White indicates statistically insignificant differences. The simulation setups are summarized in Tables 1 and A1. The flowcharts can be found in Figures 1 and A2.
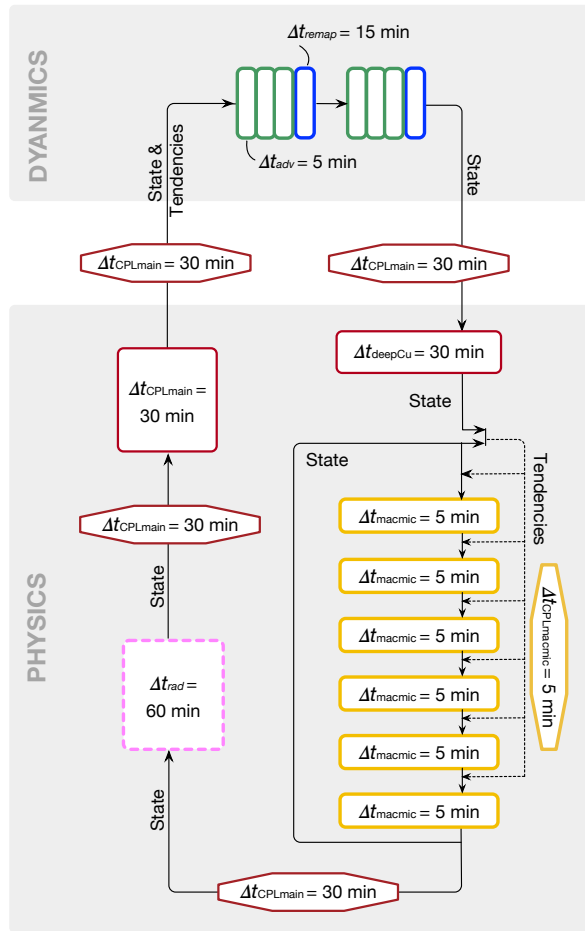
Figure 12. As in Figure 1b but for simulation v1_Dribble (cf. Tables 1 and A1).

using the simulation **v1_Dribble** which is similar to v1_CTRL but employs a revised process coupling strategy depicted in Figure 12. In the revised scheme, the atmospheric temperature, specific humidity, as well as cloud liquid and ice concentrations that are passed to the first cloud macro/microphysics subcycle are no longer the values updated by the preceding processes.

340   Instead, the older snapshot saved after the last (6th) 5 min cloud macro/microphysics subcycle in the previous main coupling time step of $\Delta t_{\mathrm{CPLmain}}$ is provided together with the corresponding total tendencies caused by all processes outside the subcycles. Before each subcycle, those tendencies are used to update the atmospheric state using a step size of $\Delta t_{\mathrm{macmic}} = 5$ min. This "dribbling" of tendencies is conceptually similar to the physics-dynamical coupling used by EAMv1's dynamical core for temperature, winds and surface pressure (Zhang et al., 2018; Rasch et al., 2019); it can be viewed as an example of the

345   sequential-tendency splitting method defined in Donahue and Caldwell (2018). To help distinguish this "dribbling" from the original sequential splitting, we introduced the notation $\Delta t_{\mathrm{CPLmacmic}}$ in Eq. (2) as well as in Table 1 and Figure 2. "Dribbling"
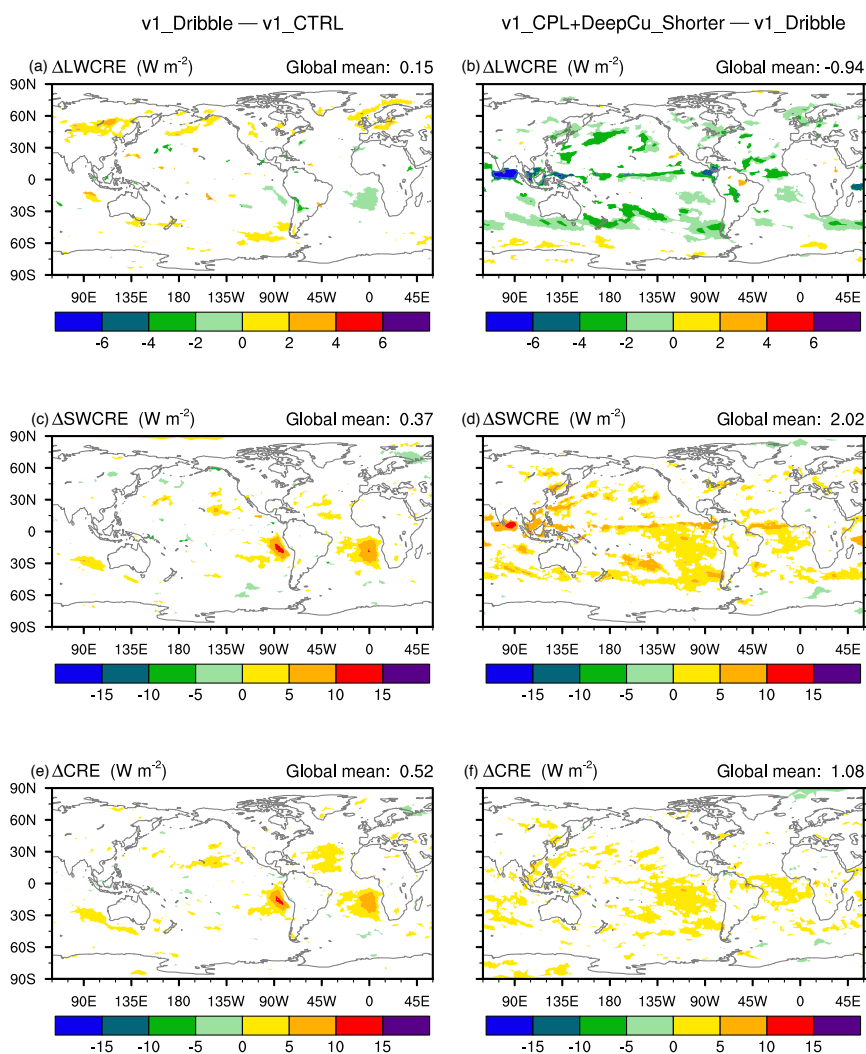
Figure 13. Attribution of the 10-year mean CRE differences shown in the left column of Figure 11. Left: differences between v1_Dribble and v1_CTRL revealing the impact of coupling between the subcycled cloud macro-/microphysics and the rest of EAM. Right: differences between v1_CPL+DeepCu_Shorter and v1_Dribble revealing the impact of step sizes used by various other parameterizations (deep convection, gravity wave drag, various aerosol processes) and the coupling among them. White indicates statistically insignificant differences. The simulation setups are summarized in Tables 1 and A1. Flowcharts are shown in Figures 1, 12, and A2b.

provides a more frequent coupling from the perspective of the subcycled cloud macro/microphysics, while the feedback to the processes outside the subcycles still occurs at longer intervals of $\Delta t_{\text{CPLmain}}$. A detailed explanation of the motivation for this "dribbling" and an in-depth analysis of its impact on the atmospheric water budget will be the topic of a separate paper. Here

350 we only show the CRE differences between the two simulations v1_Dribble and v1_CTRL (Figure 13, left column), in which weakened SWCRE and total CRE are found over the eastern parts of the subtropical oceans, especially in the regions with frequent occurrences of stratocumulus decks in the default EAMv1 model. This suggested that the strongest local reduction of SWCRE and/or total CRE seen earlier in simulations v1_All_Shorter (Figure 8d and g), v1_All_Except_MacMic_Shorter (Figure 8f and i), and v1_CPL+DeepCu_Shorter (Figure 11c and e) are primarily attributable to more frequent coupling between

355 the subcycled cloud macro/microphysics and the rest of EAM.

4.3.3 Deep convection

The simulation v1_Dribble introduced in Section 4.3.2 employed tighter coupling between the subcycled cloud macro/microphysics parameterizations but otherwise used the same step sizes as in the default model. The simulation v1_CPL+DeepCu_Shorter introduced earlier in Section 4.3.1 not only had this tighter coupling but also used 6 times shorter step sizes for other miscel-

360 laneous parameterizations and their interactions, including deep convection, land surface, gravity wave drag, aerosol sedimentation and dry deposition, as well as aerosol microphysics (but not activation). Therefore the differences in results between v1_CPL+DeepCu_Shorter and v1_Dribble provides an estimate of the impact of these other miscellaneous time steps and coupling frequencies.

Figure 13 shows the 10-year mean differences in CRE, revealing weaker LWCRE and SWCRE along the equatorial ITCZ

365 (Inter Tropical Convergence Zone, where deep convection is important) and in the subtropics and equatorward flanks of the storm tracks. The LW and SW changes largely cancel each other along the equator and near the storm tracks, leaving differences in the net CRE visible only in the trade cumulus regions. The signatures of a net cancellation in LWCRE and SWCRE along the ITCZ provide hints that there is a change in behavior in the deep convection regime. We speculate there are three possible reasons for a deep convection parameterization to be sensitive to model step size: (i) temporal truncation errors associated

370 with Δt_{deepCu}, (ii) the ratio between Δt_{deepCu} and τ where τ is the prescribed (fixed) time scale for releasing the convective available potential energy (CAPE) in the Zhang and McFarlane (1995) scheme, and (iii) the coupling between deep convection and other processes which is determined essentially by the ratio of Δt_{deepCu} to $\Delta t_{\text{CPLmain}}$; this ratio is 1 in the current EAM and in all simulations in this paper.

Williamson (2013) pointed out that convective parameterizations designed to remove instability and supersaturation on

375 assumed constant τ are constrained by Δt_{deepCu} in how much work such parameterizations can do in each time step. In contrast, large-scale condensation parameterizations designed to completely remove supersaturation within every time step are unconstrained, with implications for the column instability and depth of convection that in turn affects the resolved dynamical response. This difference in characteristic behavior can affect the simulated interactions between dynamics, deep convection and the stratiform cloud processes. Williamson (2013) showed that this time-step-time-scale issue ($\Delta t_{\text{deepCu}}/\tau$ issue) could

380 explain the occurrence of intense truncation-scale storms in high-resolution simulations conducted with the Community Atmo-
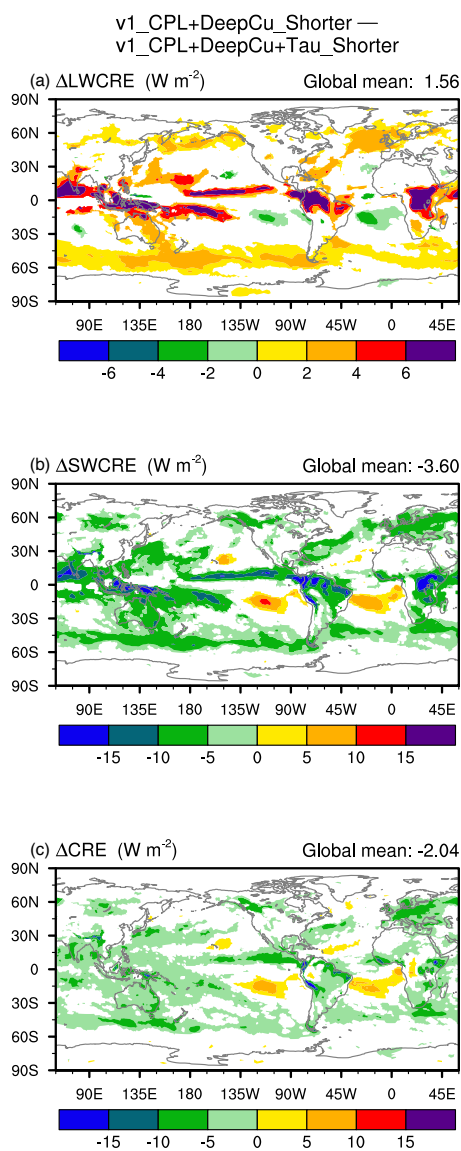
Figure 14. 10-year mean CRE differences between v1_CPL+DeepCu_Shorter and v1_CPL+DeepCu+Tau_Shorter reveal the impact of a reduced ratio of $\Delta t_{\mathrm{deepCu}}/\tau$ without model step size changes. White indicates statistically insignificant differences. The simulation setups are summarized in Tables 1 and A1. The two simulations correspond to the same flowchart shown in Figure A2b.

sphere Model Version 4 (CAM4). Other studies, e.g., Mishra et al. (2008), Mishra and Srinivasan (2010), Mishra and Sahany (2011), and Yu and Pritchard (2015), have also shown model sensitivities to $\Delta t_{\mathrm{deepCu}}$ and/or τ.

The impact of a smaller $\Delta t_{\mathrm{deepCu}}/\tau$ ratio alone, i.e., without changes in parameterization step size or process coupling frequency, can be derived by comparing the simulation v1_CPL+DeepCu_Shorter already introduced earlier and a new simulation **v1_CPL+DeepCu+Tau_Shorter** (cf. Table 1 and Figure 2, Figure A2b). The latter was configured to be identical to the former except for a different value of τ. In other words, the $\Delta t_{\mathrm{deepCu}}/\tau$ ratio is 1/6 of its default value in simulation v1_CPL+DeepCu_Shorter because of the shorter $\Delta t_{\mathrm{deepCu}}$, while the ratio was returned to its default value in EAMv1 in the new simulation v1_CPL+DeepCu+Tau_Shorter because τ was also shortened proportionally. The CRE differences between v1_CPL+DeepCu_Shorter and v1_CPL+DeepCu+Tau_Shorter, shown in Figure 14, indicate the impact of a smaller $\Delta t_{\mathrm{deepCu}}/\tau$ when model time steps and coupling frequencies remain unchanged. A smaller ratio decreases the relative importance of the convective parameterization per time step and therefore amplifies the role of the stratiform cloud parameterizations (and associated Hadley circulation); this makes the (positive) LWCRE more positive and the (negative) SWCRE more negative in convective regions. In other words, the strengthened amplitude of both LW and SW CRE in the ITCZ seen in Figure 14 is consistent with the response described in Williamson (2013).

Comparing Figure 14 with the right column of Figure 13, however, we see different signs and patterns of changes in the ITCZ. Recall that in the right column of Figure 13, the simulation v1_CPL+DeepCu_Shorter used a $\Delta t_{\mathrm{deepCu}}$ 6 times shorter than in v1_Dribble; this not only led to a smaller $\Delta t_{\mathrm{deepCu}}/\tau$ ratio but also implied that the deep convection parameterization was invoked 6 times more frequently and interacted with the resolved dynamics and other parameterized processes 6 times more frequently. The discrepancies between the right column of Figure 13 and Figure 14 suggest that the more frequent invocation of deep convection and more frequent coupling with other processes lead to consequences that compensate (in fact overcompensate) the impact of a smaller $\Delta t_{\mathrm{deepCu}}/\tau$. In other words, the overall responses of the annual mean CREs to a shortened $\Delta t_{\mathrm{deepCu}}$ is inconsistent with the time-step-time-scale discussion in Williamson (2013). Clearly, more work is needed in understanding the process interactions in the model and how these interactions respond to changes in step sizes and coupling frequencies.

5 Conclusions

This study evaluated the strength of time step sensitivities in 10-year present-day climate simulations conducted with the EAMv1 atmospheric model at 1-degree horizontal resolution. A proportional, factor-of-6 reduction of time step size in major components of the model was found to result in changes in the long-term mean climate that were significant both statistically and physically. A systematic warming was found in the low-latitude areas in the near-surface levels and a systematic cooling was seen aloft. Drying throughout the troposphere was found to be accompanied by sizable cloud fraction decreases; the primary signatures of the latter occurred at most latitudes in the upper troposphere, in the subtropical lower troposphere, and in the mid-latitude near-surface layers. In terms of geographical distribution, the most pronounced annual mean changes are the decreases in total cloud cover and CRE over the subtropical marine stratocumulus and trade cumulus regions.

The comparison of model results with a comprehensive set of observational data indicated that the changes caused by
step size reduction led to a degradation in model fidelity, in terms of both the global mean statistics and the geographical
distributions. Although this is not surprising given the careful tuning EAMv1 has gone through, the compensation of time
integration error by parameter tuning or by other sources of model error is undesirable, which also implies the need for
additional tuning to reach a new compensation when model time steps are shortened for high-resolution simulations. It would
be more desirable to identify time step algorithms with numerical errors that are small enough that the simulation fidelity is
insensitive to reasonable variations in step size; that is, so that the simulation quality is determined by physical understanding
(or lack of it).

In order to provide clues for future efforts on reducing time-stepping errors in EAM, additional simulations were con-
ducted to tease out some of the sources of time step sensitivities seen in EAMv1. Most of those simulations made use of
flexible choices of time step sizes currently available in various subsets of EAM's components. One of the simulations used
an alternate numerical scheme to couple the collectively subcycled shallow cumulus and stratiform cloud macro/microphysics
parameterizations with the rest of EAM. Another simulation used a different value for the CAPE removal time scale in the
deep convection parameterization to investigate the impact of time-step-time-scale ratio.

Analysis of the results focused mostly on annual mean cloud fraction and CRE. We found that the most notable sensitivity
in the simulations was changes in total cloud cover and CRE in the subtropical marine stratocumulus and trade cumulus
regimes. Surprisingly, we found that this sensitivity was not attributable to the step size used for treating some of the most
important processes in those regimes (turbulence, and cloud macro- and microphysical processes), but rather to the strategy
used to couple those processes to other components of the model. On the other hand, the step size of the cloud macro- and
microphysics subcycles had quite an important impact on cloud fraction at most latitudes in the upper troposphere as well as
in the mid-latitude near-surface layers. Additional simulations and analysis revealed that the deep convection parameterization
and its coupling with other processes significantly affects trade cumulus. Impacts of the step sizes used by the dynamical core
and radiation are small. In Figure A4, we have reorganized some of the CRE difference plots presented in earlier sections: a
different panel layout is used to facilitate a direct comparison of the impacts of step sizes used by different model components.
Recent follow-up or independent studies have provided insights into the impact of process coupling on marine stratocumulus
clouds and the impact of macro/microphysics time step on ice cloud formation. Those results will be reported in separate
papers. The mechanisms under the other sensitivities shown in the figure still need to be investigated.

Using the analysis method of Bony et al. (2004), we found that the subtropical low-cloud changes were primarily local,
thermodynamic responses of the model atmosphere while the impact of circulation (vertical velocity) changes was very small.
This conclusion has practical implications for follow-up investigations: since circulation changes are negligible and local cloud
processes are fast, it should be feasible to use nudged 1-year simulations (Kooperman et al., 2012; Zhang et al., 2014; Sun
et al., 2020) or even ensembles of few-day simulations (Xie et al., 2012; Ma et al., 2013; Wan et al., 2014) to help carry out
further investigations at process level and meanwhile keep the numerical experiments computationally economical.

While this study focused on one specific AGCM, we would like to advocate similar exercises be carried out with other models
as well. Based on considerations of computational cost, numerical models used for operational weather forecast and climate

research generally tend to use the longest step sizes that would provide satisfactory results. To which extent the key features

450 of those results would depend on the chosen step sizes, however, is not always clear. If a time step sensitivity quantification exercise like ours presented in Section 3 reveals strong sensitivities, that would provide a motivation to understand the causes of the sensitivities, and, in the next step, revise the numerical methods to provide higher accuracy without substantially increasing the computational cost. Root causes of time step sensitivities in comprehensive atmospheric models like EAM can be very challenging to identify due to the complex interactions and feedbacks between physical processes. Our study shows that by

455 making use of the time-stepping subcycles in a model and implementing alternate methods for process coupling, it is possible to narrow down the culprit of certain sensitivities and provide clues for further investigation and improvements.

Code availability. The EAMv0 and v1 source codes and run scripts used in this study can be found on Zenodo at https://doi.org/10.5281/zenodo.4118705.

Appendix A: Additional table and figures

460 Table A1 documents the namelist settings used in the EAMv0 and EAMv1 simulations presented in this paper to help interested readers reproduce our experiments. Figures A1 and A2 show flowcharts for sensitivity experiments conducted with EAMv1 that are not shown in Figures 1 and 12. Figure A3 presents the geographical distribution of SWCRE biases in v0_CTRL and v1_CTRL to show that the two models have different characteristics in the spatial distribution of model biases (cf. Section 3.2). In Figure A4, the CRE differences between various simulations discussed in Sections 3 and 4 are presented in a reorganized

465 layout to help highlight the conclusions of our sensitivity attribution effort.

**Table A1.** Namelist setup used by the simulations listed in Table 1.

| Group | Simulation | Description | Flowchart | Namelist variables and their values | | | | | |
				se_nsplit	rsplit	dtime	cld_macmic_num_steps	iradsw, iradlw	zmconv_tau
0	v0_CTRL	Sect. 2.2	-	2	3	1800	N/A	-1, -1	3600
I	v1_CTRL	Sect. 2.1	Fig. 1	2	3	1800	6	-1, -1	3600
I	v1_All_Shorter	Sect. 2.3	Fig. A1a	2	3	300	6	2, 2	3600
II	v1_MacMic_Shorter	Sect. 4.1	Fig. A1b	2	3	1800	36	-1, -1	3600
II	v1_All_Except_MacMic_Shorter	Sect. 4.1	Fig. A2a	2	3	300	1	2, 2	3600
III	v1_CPL+DeepCu_Shorter	Sect. 4.3.1	Fig. A2b	1	1	300	1	-1, -1	3600
III	v1_CPL+DeepCu+Tau_Shorter	Sect. 4.3.3	Fig. A2b	1	1	300	1	-1, -1	600
III	v1_Dribble	Sect. 4.3.2	Fig. 12	2	3	1800	6	-1, -1	3600
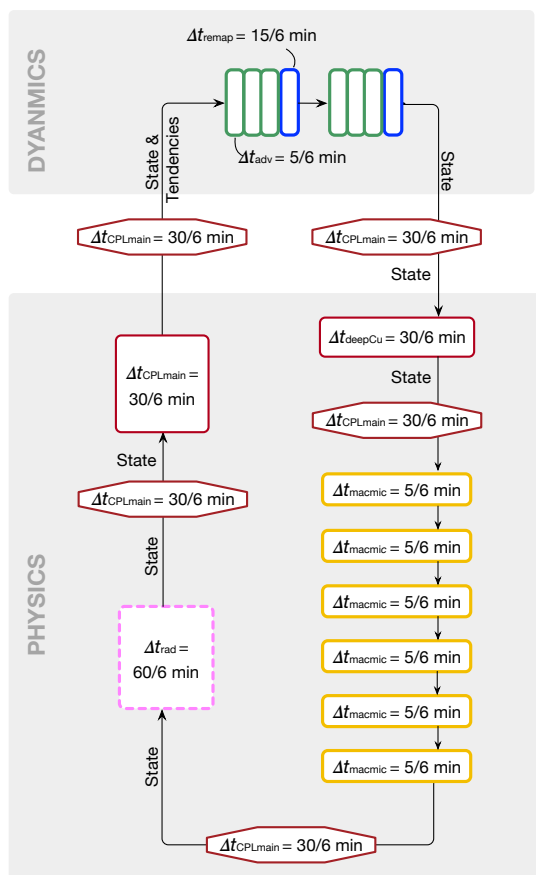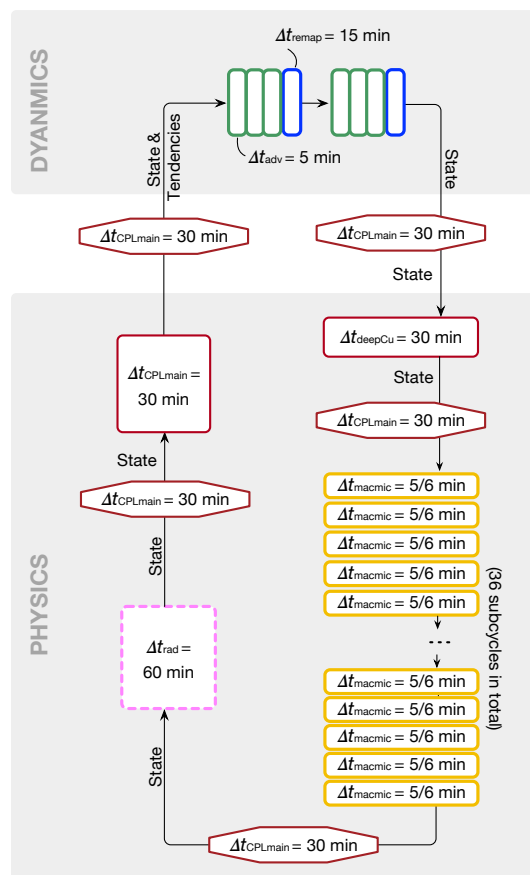
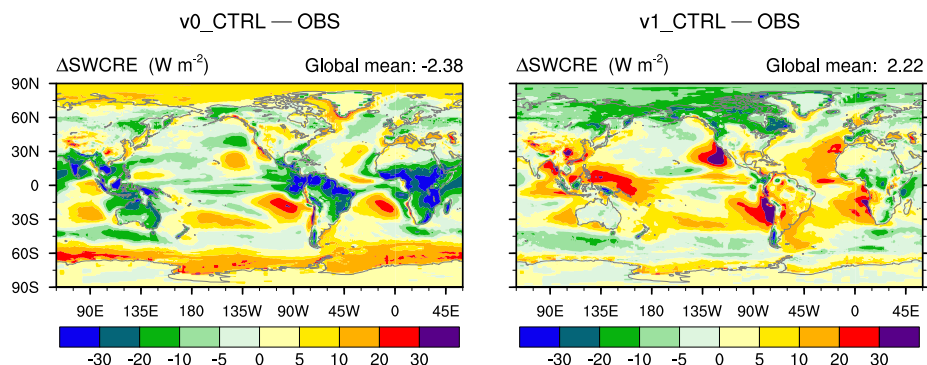**Figure A1.** As in Figures 1b and 12 but for two additional simulations listed in Tables 1 and A1.
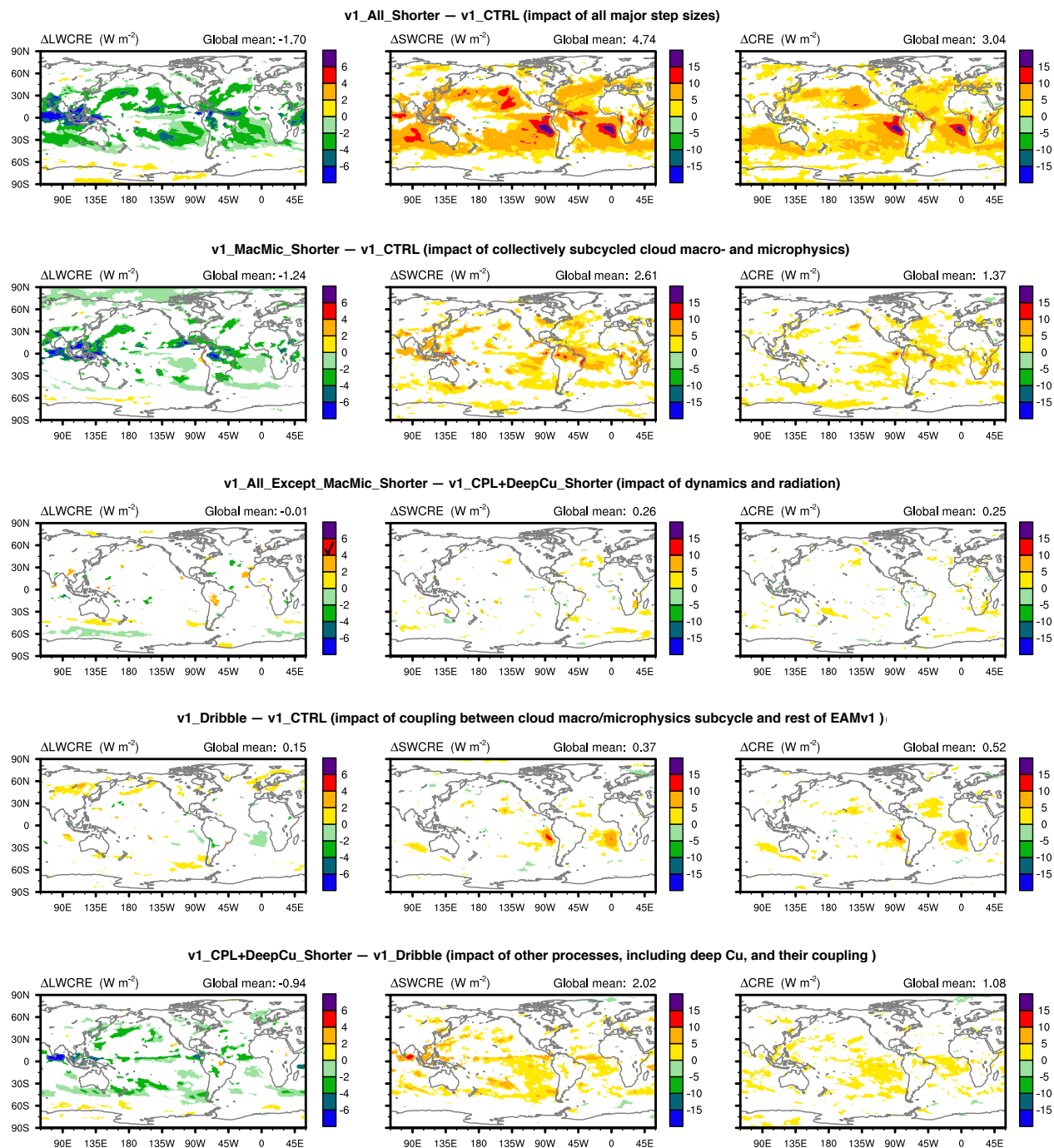
(a) v1_All_Except_MacMic_Shorter
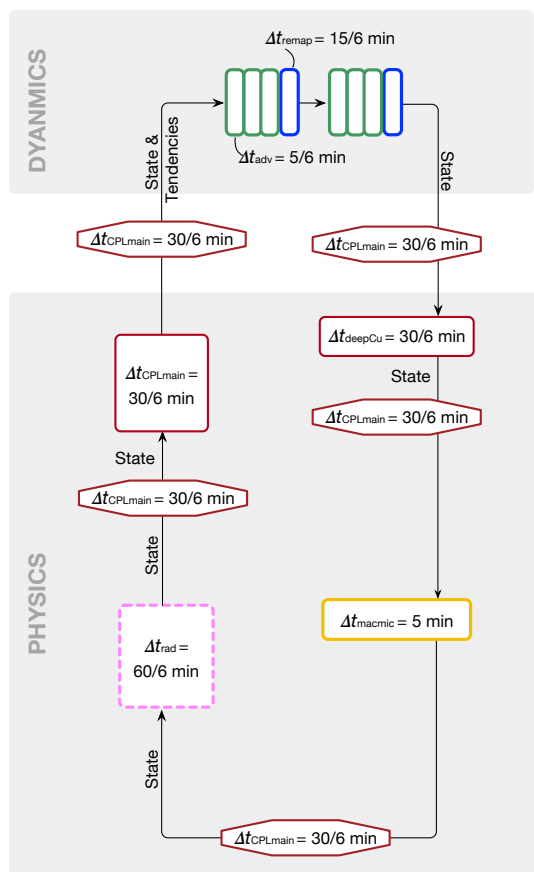
(b) v1_CPL+DeepCu_Shorter *and* v1_CPL+DeepCu+Tau_Shorter
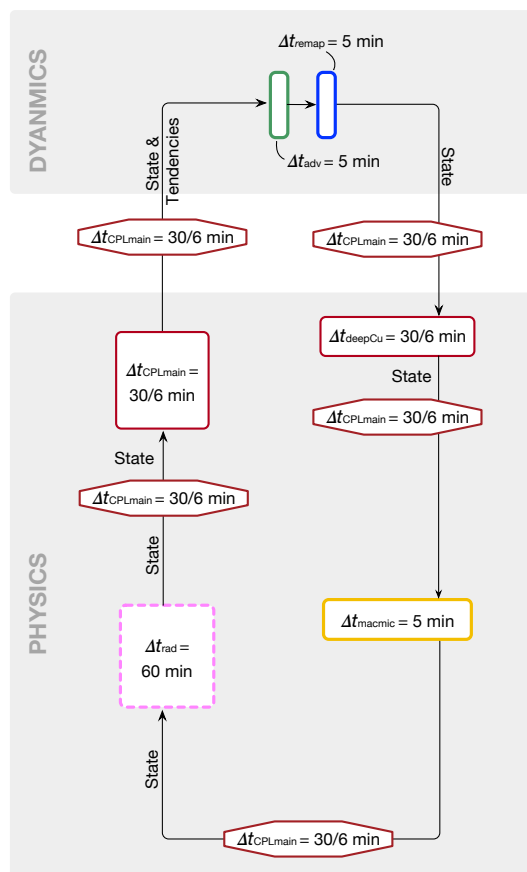
Figure A2. As in Figures 1b and 12 but for three additional simulations listed in Tables 1 and A1.

Figure A3. 10-year mean differences in SWCRE between simulations conducted with v0_CTRL (left) or v1_CTRL (right) and the 2000-2010 averages from CERES-EBAF.

Figure A4. Attribution of the 10-year mean CRE differences between v1_All_Shorter and v1_CTRL (first row) to various components of EAMv1 (lower rows). Left column: LWCRE; middle column: SWCRE; right column: total CRE. White indicates statistically insignificant differences. The attribution process is summarized in Figure 2. The simulation setups are summarized in Tables 1 and A1.

Geoscientific
Model Development
Discussions

EGU

References

Barrett, A. I., Wellmann, C., Seifert, A., Hoose, C., Vogel, B., and Kunz, M.: One Step at a Time: How Model Time Step Significantly Affects Convection-Permitting Simulations, J. Adv. Model. Earth Syst., 11, 641–658, https://doi.org/10.1029/2018MS001418, https://agupubs.onlinelibrary.wiley.com/doi/abs/10.1029/2018MS001418, 2019.

Beljaars, A.: Numerical schemes for parametrizations, in: Proceedings of the ECMWF seminar on numerical methods in atmospheric models, pp. 1–42, European Centre For Medium-Range Weather Forecasts, https://www.ecmwf.int/node/8028, 1991.

Beljaars, A., Dutra, E., Balsamo, G., and Lemarié, F.: On the numerical stability of surface–atmosphere coupling in weather and climate models, Geosci. Model Dev., 10, 977 – 989, https://doi.org/10.5194/gmd-10-977-2017, 2017.

Beljaars, A., Balsamo, G., Bechtold, P., Bozzo, A., Forbes, R., Hogan, R. J., Köhler, M., Morcrette, J.-J., Tompkins, A. M., Viterbo, P., and Wedi, N.: The Numerics of Physical Parametrization in the ECMWF Model, Frontiers in Earth Science, 6, 137, https://doi.org/10.3389/feart.2018.00137, https://www.frontiersin.org/article/10.3389/feart.2018.00137, 2018.

Bogenschutz, P. A., Gettelman, A., Morrison, H., Larson, V. E., Craig, C., and Schanen, D. P.: Higher-order turbulence closure and its impact on climate simulations in the Community Atmosphere Model, J. Clim., 26, 9655–9676, https://doi.org/10.1175/JCLI-D-13-00075.1, 2013.

Bony, S., Dufresne, J.-L., Treut, H. L., Morcrette, J.-J., and Senior, C.: On dynamic and thermodynamic components of cloud changes, Clim. Dyn., 22, 71–86, https://doi.org/10.1007/s00382-003-0369-6, 2004.

Dennis, J. M., Edwards, J., Evans, K. J., Guba, O., Lauritzen, P. H., Mirin, A. A., St-Cyr, A., Taylor, M. A., and Worley, P. H.: CAM-SE: A scalable spectral element dynamical core for the Community Atmosphere Model,, Int. J. High Perform., 26, 74–89, 2012.

Donahue, A. S. and Caldwell, P. M.: Impact of physics parameterization ordering in a global atmosphere model, J. Adv. Model. Earth Syst., 10, 481–499, https://doi.org/10.1002/2017MS001067, 2018.

Gettelman, A. and Morrison, H.: Advanced two-moment bulk microphysics for global models, Part I: Off-line tests and comparison with other schemes, Journal of Climate, 28, 1268–1287, https://doi.org/10.1175/JCLI-D-14-00102.1, 2015.

Gettelman, A., Morrison, H., Santos, S., Bogenschutz, P., and Caldwell, P. M.: Advanced Two-Moment Bulk Microphysics for Global Models. Part II: Global Model Solutions and Aerosol–Cloud Interactions*, Journal of Climate, 28, 1288–1307, https://doi.org/10.1175/JCLI-D-14-00103.1, https://doi.org/10.1175/JCLI-D-14-00103.1, 2015.

Golaz, J.-C., Larson, V., and Cotton, W.: A PDF-Based Model for Boundary Layer Clouds. Part I: Method and Model Description, J. Atmos. Sci., 59, 3540–3551, https://doi.org/10.1175/1520-0469(2002)059<3540:APBMFB>2.0.CO;2, 2002.

Guba, O., Taylor, M., and St-Cyr, A.: Optimization-based limiters for the spectral element method, J. Comput. Phys., 267, 176–195, https://doi.org/10.1016/j.jcp.2014.02.029, 2014.

Guerra, J. E. and Ullrich, P. A.: A high-order staggered finite-element vertical discretization for non-hydrostatic atmospheric models, Geoscientific Model Development, 9, 2007–2029, https://doi.org/10.5194/gmd-9-2007-2016, https://gmd.copernicus.org/articles/9/2007/2016/, 2016.

Iacono, M. J., Delamere, J. S., Mlawer, E. J., Shephard, M. W., Clough, S. A., and Collins, W. D.: Radiative forcing by long–lived greenhouse gases: Calculations with the AER radiative transfer models, J. Geophys. Res., 113, D13 103, https://doi.org/10.1029/2008JD009944, 2008.

Kinnmark, I. P. and Gray, W. G.: One step integration methods of third-fourth order accuracy with large hyperbolic stability limits, Mathematics and Computers in Simulation, 26, 181 – 188, https://doi.org/https://doi.org/10.1016/0378-4754(84)90056-9, http://www.sciencedirect.com/science/article/pii/0378475484900569, 1984.

Kooperman, G. J., Pritchard, M. S., Ghan, S. J., Wang, M., Somerville, R. C. J., and Russell, L. M.: Constraining the influence of natural variability to improve estimates of global aerosol indirect effects in a nudged version of the Community Atmosphere Model 5, Journal of Geophysical Research: Atmospheres, 117, https://doi.org/10.1029/2012JD018588, https://agupubs.onlinelibrary.wiley.com/doi/abs/10.1029/2012JD018588, 2012.

Larson, V. E. and Golaz, J.-C.: Using Probability Density Functions to Derive Consistent Closure Relationships among Higher-Order Moments, Monthly Weather Review, 133, 1023–1042, https://doi.org/10.1175/MWR2902.1, https://doi.org/10.1175/MWR2902.1, 2005.

Larson, V. E., Golaz, J.-C., and Cotton, W. R.: Small-Scale and Mesoscale Variability in Cloudy Boundary Layers: Joint Probability Density Functions, Journal of the Atmospheric Sciences, 59, 3519–3539, https://doi.org/10.1175/1520-0469(2002)059<3519:SSAMVI>2.0.CO;2, https://doi.org/10.1175/1520-0469(2002)059<3519:SSAMVI>2.0.CO;2, 2002.

Lauritzen, P. H., Nair, R. D., Herrington, A. R., Callaghan, P., Goldhaber, S., Dennis, J. M., Bacmeister, J. T., Eaton, B. E., Zarzycki, C. M., Taylor, M. A., Ullrich, P. A., Dubos, T., Gettelman, A., Neale, R. B., Dobbins, B., Reed, K. A., Hannay, C., Medeiros, B., Benedict, J. J., and Tribbia, J. J.: NCAR Release of CAM-SE in CESM2.0: A Reformulation of the Spectral Element Dynamical Core in Dry-Mass Vertical Coordinates With Comprehensive Treatment of Condensates and Energy, J. Adv. Model. Earth Syst., 10, 1537–1570, https://doi.org/10.1029/2017MS001257, https://agupubs.onlinelibrary.wiley.com/doi/abs/10.1029/2017MS001257, 2018.

Lin, S.-J.: A "Vertically Lagrangian" Finite-Volume Dynamical Core for Global Models, Mon. Wea. Rev., 132, 2293–2307, https://doi.org/10.1175/1520-0493(2004)132<2293:AVLFDC>2.0.CO;2, 2004.

Liu, X., Ma, P.-L., Wang, H., Tilmes, S., Singh, B., Easter, R. C., Ghan, S. J., and Rasch, P.: Description and evaluation of a new four–mode version of the Modal Aerosol Module (MAM4) within version 5.3 of the Community Atmosphere Model, Geosci. Model Dev., 9, 505–522, https://doi.org/doi.org/10.5194/gmd-9-505-2016, 2016.

Ma, H.-Y., Xie, S., Boyle, J. S., Klein, S. A., and Zhang, Y.: Metrics and Diagnostics for Precipitation-Related Processes in Climate Model Short-Range Hindcasts, J. Clim., 26, 1516–1534, https://doi.org/doi:10.1175/JCLI-D-12-00235.1, 2013.

Mishra, S., Srinivasan, J., and Nanjundiah, R.: The Impact of the Time Step on the Intensity of ITCZ in an Aquaplanet GCM, Mon. Wea. Rev., 136, 4077–4091, https://doi.org/10.1175/2008MWR2478.1, 2008.

Mishra, S. K. and Sahany, S.: Effects of time step size on the simulation of tropical climate in NCAR–CAM 3, Clim. Dyn., 37, 689–704, https://doi.org/10.1007/s00382-011-0994-4, 2011.

Mishra, S. K. and Srinivasan, J.: Sensitivity of the simulated precipitation to changes in convective relaxation time scale, Ann. Geophys., 28, 1827?1846, https://doi.org/10.5194/angeo-28-1827-2010, 2010.

Mlawer, E. J., Taubman, S. J., Brown, P. D., Iacono, M. J., and Clough, S. A.: Radiative transfer for inhomogeneous atmospheres: RRTM, a validated correlated?k model for the longwave, J. Geophys. Res., 102, 16,663–16,682, https://doi.org/10.1029/97JD00237, 1997.

Morrison, H. and Gettelman, A.: A New Two-Moment Bulk Stratiform Cloud Microphysics Scheme in the Community Atmosphere Model, Version 3 (CAM3). Part I: Description and Numerical Tests, J. Clim., 21, 3642–3659, https://doi.org/10.1175/2008JCLI2105.1, 2008a.

Morrison, H. and Gettelman, A.: A new two-moment bulk stratiform cloud microphysics scheme in the NCAR Community Atmosphere Model (CAM3), Part I: Description and numerical tests, J. Clim., 21, 3642–3659, https://doi.org/10.1175/2008JCLI2105.1, 2008b.

Neale, R. B., Richter, J. H., and Jochum, M.: The impact of convection on ENSO: From a delayed oscillator to a series of events, J. Clim., 21, 5904–5924, 2008.

Oleson, K., Lawrence, D., Gordon, B. B., Drewniak, B., Huang, M., Koven, C. D., Levis, S., Li, F., Riley, W. J., Subin, Z. M., Swenson, S. C., Thornton, P. E., Bozbiyik, A., Fisher, R., Heald, C. L., Kluzek, E., Lamarque, J., Lawrence, P. J., R., L. L., Sacks, W., Sun, Y.,

550   Tang, J., and Yang, Z.: Technical description of version 4.5 of the Community Land Model (CLM), NCAR technical note ncar/tn-503+str, https://doi.org/10.5065/D6RR1W7M, 2013.

Park, S. and Bretherton, C. S.: The University of Washington shallow convection and moist turbulence schemes and their impact on climate simulations with the Community Atmosphere Model, J. Clim., 22, 3449–3469, https://doi.org/10.1175/2008JCLI2557.1, 2009.

Park, S., Bretherton, C. S., and Rasch, P. J.: Integrating Cloud Processes in the Community Atmosphere Model, Version 5., J. Clim., 27,
555   6821–6855, https://doi.org/10.1175/JCLI-D-14-00087.1, 2014.

Rasch, P. J., Xie, S., Ma, P.-L., Lin, W., Wang, H., Tang, Q., Burrows, S. M., Caldwell, P., Zhang, K., Easter, R. C., Cameron-Smith, P., Singh, B., Wan, H., Golaz, J.-C., Harrop, B. E., Roesler, E., Bacmeister, J., Larson, V. E., Evans, K. J., Qian, Y., Taylor, M., Leung, L. R., Zhang, Y., Brent, L., Branstetter, M., Hannay, C., Mahajan, S., Mametjanov, A., Neale, R., Richter, J. H., Yoon, J.-H., Zender, C. S., Bader, D., Flanner, M., Foucar, J. G., Jacob, R., Keen, N., Klein, S. A., Liu, X., Salinger, A., Shrivastava, M., and Yang, Y.: An Overview of the
560   Atmospheric Component of the Energy Exascale Earth System Model, Journal of Advances in Modeling Earth Systems, 11, 2377–2411, https://doi.org/10.1029/2019MS001629, https://agupubs.onlinelibrary.wiley.com/doi/abs/10.1029/2019MS001629, 2019.

Richter, J. H. and Rasch, P. J.: Effects of Convective Momentum Transport on the Atmospheric Circulation in the Community Atmosphere Model, Version 3, J. Clim., 21, 1487–1499, https://doi.org/10.5194/gmd-10-2221-2017, 2008.

Spiteri, R. J. and Ruuth, S. J.: A New Class of Optimal High-Order Strong-Stability-Preserving Time Discretization Methods, SIAM J.
565   Numer. Anal., 40, 469–491, https://doi.org/10.1137/S0036142901389025, 2002.

Sportisse, B.: An Analysis of Operator Splitting Techniques in the Stiff Case, Journal of Computational Physics, 161, 140 – 168, https://doi.org/https://doi.org/10.1006/jcph.2000.6495, http://www.sciencedirect.com/science/article/pii/S0021999100964957, 2000.

Sun, J., Zhang, K., Wan, H., Ma, P.-L., Tang, Q., and Zhang, S.: Impact of Nudging Strategy on the Climate Representativeness and Hindcast Skill of Constrained EAMv1 Simulations, Journal of Advances in Modeling Earth Systems, n/a, https://doi.org/10.1029/2019MS001831,
570   https://agupubs.onlinelibrary.wiley.com/doi/abs/10.1029/2019MS001831, 2020.

Taylor, M. A., Cyr, A. S., and Fournier, A.: A Non-oscillatory Advection Operator for the Compatible Spectral Element Method,, International Conference on Computational Science, Springer, Berlin, Heidelberg, https://doi.org/10.1007/978-3-642-01973-9_31, 2009.

Wan, H., Rasch, P. J., Zhang, K., Kazil, J., and Leung, L. R.: Numerical issues associated with compensating and competing processes in climate models: an example from ECHAM-HAM, Geosci. Model Dev., 6, 861–874, https://doi.org/10.5194/gmd-6-861-2013, https:
575   //www.geosci-model-dev.net/6/861/2013/, 2013.

Wan, H., Rasch, P. J., Zhang, K., Qian, Y., Yan, H., and Zhao, C.: Short ensembles: an efficient method for discerning climate-relevant sensitivities in atmospheric general circulation models, Geosci. Model Dev., 7, 1961–1977, https://doi.org/10.5194/gmd-7-1961-2014, 2014.

Wang, H., Easter, R. C., Zhang, R., Ma, P.-L., Singh, B., Zhang, K., Ganguly, D., Rasch, P. J., Burrows, S. M., Ghan, S. J., Lou, S., Qian,
580   Y., Yang, Y., Feng, Y., Flanner, M., Leung, R. L., Liu, X., Shrivastava, M., Sun, J., Tang, Q., Xie, S., and Yoon, J.-H.: Aerosols in the E3SM Version 1: New Developments and Their Impacts on Radiative Forcing, Journal of Advances in Modeling Earth Systems, 12, e2019MS001 851, https://doi.org/10.1029/2019MS001851, 2020.

Wang, Y., Liu, X., Hoose, C., and Wang, B.: Different contact angle distributions for heterogeneous ice nucleation in the Community Atmospheric Model version 5,, Atmos. Chem. Phys., 14, 10 411–10 430, https://doi.org/doi.org/10.5194/acp-14-10411-2014, 2014.

585   Williamson, D. L.: Time-Split versus Process-Split Coupling of Parameterizations and Dynamical Core, Monthly Weather Review, 130, 2024–2041, http://dx.doi.org/10.1175/1520-0493(2002)130<2024:TSVPSC>2.0.CO;2, 2002.

Williamson, D. L.: The effect of time steps and time-scales on parametrization suites, Q. J. R. Meteorol. Soc., 139, 548 – 560, https://doi.org/10.1002/qj.1992, 2013.

Xie, S., Ma, H.-Y., Boyle, J. S., Klein, S. A., and Zhang, Y.: On the Correspondence between Short- and Long-Time-Scale Systematic Errors
590   in CAM4/CAM5 for the Year of Tropical Convection, Journal of Climate, 25, 7937–7955, https://doi.org/10.1175/JCLI-D-12-00134.1, https://doi.org/10.1175/JCLI-D-12-00134.1, 2012.

Xie, S., Lin, W., Rasch, P. J., Ma, P., Neale, R., Larson, V. E., Qian, Y., Bogenschutz, P. A., Caldwell, P., Cameron?Smith, P., Golaz, J., Maha-jan, S., Singh, B., Tang, Q., Wang, H., Yoon, J., Zhang, K., and Zhang, Y.: Understanding cloud and convective characteristics in version 1 of the E3SM atmosphere model, J. Adv. Model. Earth Syst., 10, 2618–2644, https://doi.org/https://doi.org/10.1029/2018MS001350, 2018.

595   Yu, S. and Pritchard, M. S.: The effect of large-scale model time step and multiscale coupling frequency on cloud clima-tology, vertical structure, and rainfall extremes in a superparameterized GCM, J. Adv. Model. Earth Syst., 7, 1977–1996, https://doi.org/10.1002/2015MS000493., 2015.

Zhang, G. J. and McFarlane, N. A.: Sensitivity of climate simulations to the parameterization of cumulus convection in the Canadian Climate Centre general circulation model, Atmos. Ocean, 33, 407–446, https://doi.org/10.1080/07055900.1995.9649539, 1995.

600   Zhang, K., Wan, H., Liu, X., Ghan, S. J., Kooperman, G. J., Ma, P.-L., Rasch, P. J., Neubauer, D., and Lohmann, U.: Technical Note: On the use of nudging for aerosol–climate model intercomparison studies, Atmospheric Chemistry and Physics, 14, 8631–8645, https://doi.org/10.5194/acp-14-8631-2014, https://www.atmos-chem-phys.net/14/8631/2014/, 2014.

Zhang, K., Rasch, P. J., Taylor, M. A., Wan, H., Leung, R., Ma, P.-L., Golaz, J.-C., Wolfe, J., Lin, W., Singh, B., Burrows, S., Yoon, J.-H., Wang, H., Qian, Y., Tang, Q., Caldwell, P., and Xie, S.: Impact of numerical choices on water conservation in the E3SM Atmosphere
605   Model version 1 (EAMv1), Geosci. Model Dev., 11, 1971–1988, https://doi.org/10.5194/gmd-11-1971-2018, 2018.

Zwiers, F. W. and von Storch, H.: Taking Serial Correlation into Account in Tests of the Mean, Journal of Climate, 8, 336–351, https://doi.org/10.1175/1520-0442(1995)008<0336:TSCIAI>2.0.CO;2, https://doi.org/10.1175/1520-0442(1995)008<0336: TSCIAI>2.0.CO;2, 1995.